C. Tantos, D. Valougeorgis, A. Frezzotti
Conductive Heat Transfer in Rarefied Polyatomic Gases Confined Between Parallel Plates via Various Kinetic Models and the DSMC Method
International Journal of Heat and Mass Transfer, Vol. 88, 2015, p. 636-651
doi:10.1016/j.ijheatmasstransfer.2015.04.092

Conductive heat transfer in rarefied polyatomic gases confined between parallel plates via various kinetic models and the DSMC method

Christos Tantos[1], Dimitris Valougeorgis[1*], Aldo Frezzotti[2]

[1]Department of Mechanical Engineering, University of Thessaly, 38334 Volos, Greece

[2]Dipartimento di Scienze & Tecnologie Aerospaziali, Politecnico di Milano, 20156 Milano, Italy

Abstract

The conductive heat transfer through rarefied polyatomic gases confined between parallel plates maintained at different temperatures is investigated. The approach is based on three kinetic models namely the Holway, Rykov and Andries models, as well on the DSMC scheme supplemented by the Borgnakke-Larsen collision model. Results are presented for the total as well as for the translational and rotational parts of the heat flux and of the density and temperature fields in a wide range of the Knudsen number and for small, moderate and large temperature differences. The effect of the thermal accommodation at the boundaries is also examined for two diffuse-specular reflection scenarios at the walls. All three kinetic models provide results which are in very good agreement between them and they also compare very well with corresponding DSMC results. Comparisons with experimental results are performed verifying the validity of the simulations. The total heat fluxes of diatomic and polyatomic gases have been found to be about 30–50% and 50–75% respectively higher than the corresponding monatomic ones, with the highest differences occurring in the free molecular limit. The translational and rotational temperature distributions (as well as the total temperature) are very close to each other for each set of parameters examined and they are close to the corresponding monatomic ones, when the translational and rotational accommodation coefficients are the same. On the contrary they depart from each other when the two coefficients are different. In most cases as the gas-surface interaction becomes more diffusive the dimensionless total heat flux is monotonically increased. However, for adequately large temperature differences and sufficiently high gas rarefaction levels a non-monotonic behavior has been observed. It has been also found that in polyatomic gases the dimensional heat flux is not necessarily increased as the molar mass is decreased, which is always the case in monatomic gases.

Keywords: Kinetic theory, Polyatomic kinetic modeling, DSMC, Rotational degrees of freedom, Micro heat transfer, Vacuum technology, Pirani sensor.

[*] Corresponding author: diva@mie.uth.gr

1. Introduction

Heat transfer through stationary rarefied gases confined between solid surfaces continues to be an active area of research [1,2,3,4]. This is well justified since this heat transfer configuration is very common in several technological applications including vacuum pressure gauges [5], vacuum solar collectors [6], multilayer insulation blankets in space and cryogenic equipment [7], micro heat exchangers and microsensors [8,9]. It is also commonly used as a prototype set-up in order to determine the thermal conductivity of gases [10] the temperature jump coefficient [11] and the energy accommodation at the cold and hot surfaces, combining modeling and measurements [12,13,14].

Heat transfer modelling in rarefied gases is commonly based on kinetic theory [15,16] in order to yield reliable solutions in the whole range of the Knudsen number in a unified manner. Although the kinetic theory of plane and cylindrical heat conduction has been extensively applied to monatomic gases, the corresponding problem for polyatomic gases has received considerable less attention mainly due to the increased complexity in the intermolecular collision [17] and the molecular-wall interaction [18] processes. Most of the available work is based on the Morse [19], Holway [20] and Hanson & Morse [21] polyatomic kinetic models and it is mainly focused in small temperature differences. Then, the problem is treated via linearized kinetic analysis and the governing equations are solved by variational methods [22] or by transforming the boundary value problem into a system of integral equations. Following this latter approach extensive results have been provided in [23] for the heat fluxes through several polyatomic gases confined between parallel plates in terms of the Knudsen number and the thermal accommodation coefficients for translational and rotational energy.

Similar work in the case of large temperature differences is very limited. Nonlinear heat transfer in diatomic gases has been solved based on the Holway model in [24] and more recently in [18] based on the model proposed by Rykov [25,26]. In both cases the solution is based on versions of the discrete ordinates (velocity) method, while good agreement with experimental results [27,28,13] has been observed. In [18] the work is focused on the influence of the boundary conditions on the macroscopic quantities. Very recently, based on the Holway and Rykov models as well as on the DSMC method, an extended description of heat transfer in rarefied polyatomic gases between coaxial cylinders has been provided in [29].

In the present work a detailed computational investigation of conductive heat transfer through rarefied polyatomic gases confined between parallel plates is performed providing a complete description of the heat flux and temperature and density distributions in terms of all involved parameters. The formulation is based on the kinetic models proposed by Holway and Rykov as well as on the more recently introduced model by Andries et al. [30]. In addition, the solution is also obtained by the Boltzmann equation via the DSMC scheme supplemented by the Borgnakke-Larsen collision model [31]. A systematic comparison between the results obtained by the three kinetic models and the DSMC method, by ensuring equivalent translational and rotational relaxation rates, is performed. The effect of the thermal accommodation at the boundaries is also examined for various diffuse-specular reflection scenarios at the walls and a comparison with corresponding experimental work is included. Overall, the influence of the number of rotational degrees of freedom is investigated and the differences (and similarities) compared to the corresponding monatomic gas heat transfer problem are pointed out.

2. Heat transfer configuration and main definitions

Consider a stationary polyatomic gas confined between two infinite parallel plates, fixed at $\hat{y} = \pm H/2$ and maintained at constant temperatures T_H and T_C respectively, with $T_H > T_C$. Then, due to the temperature difference, a steady one-dimensional heat flow is established in the direction normal to the plates and directed from the hot towards the cold plate. The present analysis treats only the translational and rotational energy modes ignoring the vibrational ones. Depending on the desired accuracy level, vibrational excitation must be included when the flow characteristic temperature exceeds 25-30% of the gas characteristic vibrational temperature which varies significantly for each gas. For instance, for O_2 and N_2 the characteristic vibrational temperatures are 2256K and 3371K respectively, whereas for CO_2 is 960K.

In the temperature range where the effects of vibrational degrees of freedom can be neglected, the problem may be modeled by the Boltzmann equation for a gas of rigid rotators. When intrinsic molecular angular momenta (spin) has no preferential alignment, the gas may be described by a spin orientation averaged distribution function $\hat{f}\left(\hat{y}, \boldsymbol{v}, \hat{I}\right)$, where $\boldsymbol{v} = \left(\xi_x, \xi_y, \xi_z\right)$ is the molecular velocity vector and $\hat{I}$ is the internal energy, describing the molecular internal states through a single variable [17].

In polyatomic gases the internal energy can be divided in two parts, the energy of the translational motion and the energy associated to the internal structure. These energies are related to the corresponding so-called translational and rotational temperatures and heat fluxes. Then, the macroscopic quantities of practical interest are obtained by the moments of $\hat{f}$ as

$$n(\hat{y}) = \int_{-\infty}^{\infty}\int_{-\infty}^{\infty}\int_{-\infty}^{\infty}\int_{0}^{\infty} \hat{f} d\hat{I} d\xi_x d\xi_y d\xi_z \,, \tag{1}$$

$$T_{tr}(\hat{y}) = \frac{m}{3k_B n}\int_{-\infty}^{\infty}\int_{-\infty}^{\infty}\int_{-\infty}^{\infty}\int_{0}^{\infty} \upsilon^2 \hat{f} d\hat{I} d\xi_x d\xi_y d\xi_z \,, \qquad T_{rot}(\hat{y}) = \frac{2}{jk_B n}\int_{-\infty}^{\infty}\int_{-\infty}^{\infty}\int_{-\infty}^{\infty}\int_{0}^{\infty} \hat{I}\hat{f} d\hat{I} d\xi_x d\xi_y d\xi_z \tag{2}$$

$$T(\hat{y}) = \frac{3T_{tr}(\hat{y}) + jT_{rot}(\hat{y})}{3+j}, \tag{3}$$

$$Q_{tr}(\hat{y}) = \frac{m}{2}\int_{-\infty}^{\infty}\int_{-\infty}^{\infty}\int_{-\infty}^{\infty}\int_{0}^{\infty} \xi_y \upsilon^2 \hat{f} d\hat{I} d\xi_x d\xi_y d\xi_z \,, \qquad Q_{rot}(\hat{y}) = \int_{-\infty}^{\infty}\int_{-\infty}^{\infty}\int_{-\infty}^{\infty}\int_{0}^{\infty} \xi_y \hat{I}\hat{f} d\hat{I} d\xi_x d\xi_y d\xi_z \tag{4}$$

$$Q(\hat{y}) = Q_{tr}(\hat{y}) + Q_{rot}(\hat{y}), \tag{5}$$

$$\tilde{P}_{ii}(\hat{y}) = m\int_{-\infty}^{\infty}\int_{-\infty}^{\infty}\int_{-\infty}^{\infty}\int_{0}^{\infty} \xi_i^2 \hat{f} d\hat{I} d\xi_x d\xi_y d\xi_z \,, \qquad i = x, y, z \tag{6}$$

where n, T, Q and $\tilde{P}_{ii}$ are the number density, total (thermodynamic) temperature, total heat flux and normal stresses respectively. The subscripts *tr* and *rot* denote the translational and rotational parts, while the parameter j is the number of rotational degrees of freedom, with $j = 2$ for diatomic and linear molecules and $j = 3$ in all other cases ($j = 0$ refers to monoatomic molecules).

The main two parameters characterizing the problem are the normalized temperature difference

$$\beta = \frac{T_H - T_C}{2T_0} \tag{7}$$

where $T_0 = (T_H + T_C)/2$ is the reference temperature and the reference gas rarefaction parameter

$$\delta_0 = \frac{P_0 H}{\mu_0 \upsilon_0} \tag{8}$$

In Eq. (8), μ_0 is the gas viscosity at reference temperature T_0, $\upsilon_0 = \sqrt{2k_B T_0 / m}$ with k_B being the Boltzmann constant and m the molecular mass, is the most probable molecular speed and

$P_0 = n_0 k_B T_0$, with $n_0 = \frac{1}{H}\int_{-H/2}^{H/2} n(\hat{y})\, d\hat{y}$, is a reference pressure. It is noted that $\delta_0 \in [0,\infty)$ and it is proportional to the inverse Knudsen number, with the limiting values of $\delta_0 = 0$ and $\delta_0 \to \infty$ corresponding to the free molecular and hydrodynamic limits respectively. In addition to the parameters β and δ_0 the problem is also characterized by the type of wall-gas interaction, which is defined in Section 3.3.

Furthermore, it is convenient to introduce the following dimensionless variables and macroscopic quantities:

$$y = \hat{y}/H,\ \boldsymbol{c} = \boldsymbol{v}/v_0,\ I = \hat{I}/k_B T_0,\ f = \hat{f} v_0^3 k_B T_0 / n_0 \tag{9}$$

$$\rho = n/n_0,\ P_{ii} = \tilde{P}_{ii}/(2 n_0 k_B T_0) \tag{10}$$

$$\tau_{tr} = T_{tr}/T_0,\ \tau_{rot} = T_{rot}/T_0,\ \tau = (3\tau_{tr} + j\tau_{rot})/(3+j) \tag{11}$$

$$q_{tr} = Q_{tr}/(n_0 k_B T_0 v_0),\ q_{rot} = Q_{rot}/(n_0 k_B T_0 v_0),\ q = q_{tr} + q_{rot} \tag{12}$$

Here, the effect of all parameters on the translational and rotational heat fluxes and temperature distributions as well as on the density distribution for polyatomic gases is examined. This is achieved both in a deterministic and stochastic manner described in Sections 3 and 4 respectively.

3. Polyatomic kinetic modeling

The effort of solving the Boltzmann equation either analytically or numerically, is significantly reduced by substituting its collision term with reliable kinetic models. The two well-known models introduced by Holway [20] and Rykov [25,26] as well as the more recently introduced model by Andries [30], are implemented. All three models may be considered as BGK type models and, for monatomic gases they are reduced to the BGK [32], Shakhov [33] and ES [20] models respectively. The models by Holway and Rykov, where the collision integral consists of two components corresponding to the elastic and inelastic collisions are described in Section 3.1. The model by Andries, where the collision term is kept in compact form as it is in the ES model with a new "artificial" temperature which is accordingly decomposed into translational and rotational parts, is provided in Section 3.2. The associated boundary conditions are given in Section 3.3, while the translational and rotational relaxation rates of all models are formulated in the Appendix A. The H-theorem has been proved in [30] for the Andries model

and can be proved in a straightforward manner for the Holway model following the arguments leading to analogous proof of the BGK model.

It is obvious that the dependency of the distribution function f on the energy I of the rotational motion significantly increases the computational effort compared to the monatomic gas case. However, for BGK type models all macroscopic quantities can be obtained by a simpler formalism introducing two reduced density distributions one for the mass and one for the internal energy according to $g=\int_0^\infty f dI$ and $h=\int_0^\infty f I dI$ [18,30,34]. For the specific problem under consideration the computational effort is further reduced by eliminating, based on the so-called projection procedure, the c_x and c_z components of the molecular velocity by introducing the reduced distributions:

$$F^{(i)}\left(y,c_y\right)=\int_{-\infty}^{\infty}\int_{-\infty}^{\infty} g dc_z dc_x,\ G^{(i)}\left(y,c_y\right)=\int_{-\infty}^{\infty}\int_{-\infty}^{\infty} g\left(c_z^2+c_x^2\right) dc_z dc_x,\ S^{(i)}\left(y,c_y\right)=\int_{-\infty}^{\infty}\int_{-\infty}^{\infty} h dc_z dc_x,$$

$$R^{(i)}\left(y,c_y\right)=\int_{-\infty}^{\infty}\int_{-\infty}^{\infty} g c_x^2 dc_z dc_x \tag{13}$$

In Eq. (13) the superscript $i=H,R,A$ denotes the Holway (H), Rykov (R) and Andries (A) models respectively. By operating accordingly with the appropriate integral operators on the original form of each of the kinetic model equations the corresponding reduced systems of integro-differential equations for each model may be obtained.

3.1 Models with elastic and inelastic collision terms

The Holway and Rykov models, which have been commonly applied with considerable success in rarefied polyatomic gas flows and heat transfer configurations [26,29,34,35,36], are formulated. For the present one-dimensional heat transfer problem both models may be written in a similar compact form as

$$c_y\frac{\partial \boldsymbol{\Psi}^{(i)}}{\partial y}=\delta_0\rho^{(i)}\left(\tau_{tr}^{(i)}\right)^{1-\omega}\mathrm{Pr}^{\chi}\left[\frac{1}{Z^{(i)}}\left(\boldsymbol{\Psi}_{rot}^{(i)}-\boldsymbol{\Psi}^{(i)}\right)+\left(1-\frac{1}{Z^{(i)}}\right)\left(\boldsymbol{\Psi}_{tr}^{(i)}-\boldsymbol{\Psi}^{(i)}\right)\right] \tag{14}$$

where $i=H,R$. Here, the vector of the unknown distributions $\boldsymbol{\Psi}^{(i)}=\left[F^{(i)},G^{(i)},S^{(i)}\right]^T$ depends on two independent variables, namely y and c_y. Also, the reference gas rarefaction δ_0 is given by Eq. (8), Pr is the Prandtl number of the gas, with the parameter $\chi=1$ in the Holway model

and $\chi = 0$ in the Rykov model, while the parameter $1 \le Z^{(i)} < \infty$ indicates the fraction of rotational collisions with regard to the total collisions. As $Z^{(i)} \to \infty$, the first two equations in (14) for $i = H, R$ are transformed to the corresponding reduced BGK and Shakhov equations for monatomic gas. In the derivation of Eq. (14) the Inverse Power Law (IPL) interaction between particles has been introduced with $\omega \in [1/2, 1]$.

The translational and rotational relaxing distributions in Eq. (14) are given by $\boldsymbol{\Psi}_{tr}^{(i)} = \left[F_{tr}^{(i)}, G_{tr}^{(i)}, S_{tr}^{(i)} \right]^T$ and $\boldsymbol{\Psi}_{rot}^{(i)} = \left[F_{rot}^{(i)}, G_{rot}^{(i)}, S_{rot}^{(i)} \right]^T$ respectively, where the components of these vectors for each kinetic model are as follows:

- Holway model

$$F_{tr}^{(H)} = \frac{\rho^{(H)}}{\sqrt{\pi \tau_{tr}^{(H)}}} \exp\left[-c_y^2 / \tau_{tr}^{(H)} \right] \qquad G_{tr}^{(H)} = \tau_{tr}^{(H)} F_{tr}^{(H)} \qquad S_{tr}^{(H)} = \frac{j}{2} \tau_{rot}^{(H)} F_{tr}^{(H)}$$

$$F_{rot}^{(H)} = \frac{\rho^{(H)}}{\sqrt{\pi \tau_{tr}^{(H)}}} \exp\left[-c_y^2 / \tau^{(H)} \right] \qquad G_{rot}^{(H)} = \tau^{(H)} F_{rot}^{(H)} \qquad S_{rot}^{(H)} = \frac{j}{2} \tau^{(H)} F_{rot}^{(H)} \qquad (15)$$

- Rykov model

$$F_{tr}^{(R)} = \frac{\rho^{(R)}}{\sqrt{\pi \tau_{tr}^{(R)}}} \exp\left[-\frac{c_y^2}{\tau_{tr}^{(R)}} \right] \left[1 + \frac{4}{15} \frac{q_{tr}^{(R)} c_y}{\rho^{(R)} \left(\tau_{tr}^{(R)} \right)^2} \left(\frac{c_y^2}{\tau_{tr}^{(R)}} - \frac{3}{2} \right) \right]$$

$$G_{tr}^{(R)} = \frac{\rho^{(R)} \sqrt{\tau_{tr}^{(R)}}}{\sqrt{\pi}} \exp\left[-\frac{c_y^2}{\tau_{tr}^{(R)}} \right] \left[1 + \frac{4}{15} \frac{q_{tr}^{(R)} c_y}{\rho^{(R)} \left(\tau_{tr}^{(R)} \right)^2} \left(\frac{c_y^2}{\tau_{tr}^{(R)}} - \frac{1}{2} \right) \right]$$

$$S_{tr}^{(R)} = \frac{\rho^{(R)} \tau_{rot}^{(R)}}{\sqrt{\pi \tau_{tr}^{(R)}}} \exp\left[-\frac{c_y^2}{\tau_{tr}^{(R)}} \right] \left[1 + \frac{4}{15} \frac{q_{tr}^{(R)} c_y}{\rho^{(R)} \left(\tau_{tr}^{(R)} \right)^2} \left(\frac{c_y^2}{\tau_{tr}^{(R)}} - \frac{3}{2} \right) + 2(1-\kappa) \frac{q_{rot}^{(R)} c_y}{\rho^{(R)} \tau_{tr}^{(R)} \tau_{rot}^{(R)}} \right]$$

$$F_{rot}^{(R)} = \frac{\rho^{(R)}}{\sqrt{\pi \tau^{(R)}}} \exp\left[-\frac{c_y^2}{\tau^{(R)}} \right] \left[1 + \varpi_0 \frac{4}{15} \frac{q_{tr}^{(R)} c_y}{\rho^{(R)} \left(\tau^{(R)} \right)^2} \left(\frac{c_y^2}{\tau^{(R)}} - \frac{3}{2} \right) \right]$$

$$G_{rot}^{(R)} = \frac{\rho^{(R)} \sqrt{\tau^{(R)}}}{\sqrt{\pi}} \exp\left[-\frac{c_y^2}{\tau^{(R)}} \right] \left[1 + \varpi_0 \frac{4}{15} \frac{q_{tr}^{(R)} c_y}{\rho^{(R)} \left(\tau^{(R)} \right)^2} \left(\frac{c_y^2}{\tau^{(R)}} - \frac{1}{2} \right) \right]$$

$$S_{rot}^{(R)}=\frac{\rho^{(R)}\sqrt{\tau^{(R)}}}{\sqrt{\pi}}\exp\left[-\frac{c_y^2}{\tau^{(R)}}\right]\left[1+\varpi_0\frac{4}{15}\frac{q_{tr}^{(R)}c_y}{\rho^{(R)}\left(\tau^{(R)}\right)^2}\left(\frac{c_y^2}{\tau^{(R)}}-\frac{3}{2}\right)+2\varpi_1\left(1-\kappa\right)\frac{q_{rot}^{(R)}c_y}{\rho^{(R)}\left(\tau^{(R)}\right)^2}\right] \quad (16)$$

The Holway model cannot recover the shear viscosity and thermal conductivity simultaneously and since here a purely heat transfer configuration is investigated the collision frequency has been set to properly recover the property of thermal conductivity. The Rykov model, as the Shakhov model for monatomic gases, recovers both coefficients. The parameter $\kappa=\mu/\left(mnD\right)$, where D is the gas self-diffusion coefficient, is a constant which for a power intermolecular potential is varying between the values of 1/1.2 for hard spheres and 1/1.543 for Maxwell molecules [26,37]. It is also stated in [26] that the parameters ϖ_0 and ϖ_1 are chosen so that the thermal conductivity obtained from the model equation is close to the experimental data in [38]. Alternatively, following the theory in [39], once the constant κ and the rotational collision number $Z^{(R)}$ are defined, the parameters ϖ_0 and ϖ_1 may be determined in order to obtain the correct translational and rotational thermal conductivity coefficients from the equations [39,40]:

$$\left(1+\frac{1-\varpi_0}{2Z^{(R)}}\right)^{-1}=1-\frac{1}{2Z^{(R)}}\left(1-\frac{2}{5\kappa}\right) \qquad \left(1+\frac{\left(1-\kappa\right)\left(1-\varpi_1\right)}{Z^{(R)}\kappa}\right)^{-1}=1+\frac{3}{4Z^{(R)}}\left(1-\frac{2}{5\kappa}\right) \quad (17)$$

Then, based on Eqs. (17), the Prandtl number is given by [40]

$$\mathrm{Pr}=\frac{7}{5Z^{(R)}}\left[\frac{3}{2Z^{(R)}+1-\varpi_0}+\frac{0.4}{\kappa Z^{(R)}+\left(1-\kappa\right)\left(1-\varpi_1\right)}\right]^{-1}. \quad (18)$$

In cases where the Pr number, along with the constant κ and the collision number $Z^{(R)}$, are given, Eq. (18) and either of Eqs. (17) may be used to define ϖ_0 and ϖ_1.

The dimensionless macroscopic quantities in terms of the reduced distributions $F^{(i)}$, $G^{(i)}$ and $S^{(i)}$ are given by the following moments:

$$\rho^{(i)}=\int_{-\infty}^{\infty}F^{(i)}dc_y \quad (19)$$

$$\tau_{tr}^{(i)}=\frac{2}{3\rho^{(i)}}\int_{-\infty}^{\infty}\left(c_y^2F^{(i)}+G^{(i)}\right)dc_y \qquad \tau_{rot}^{(i)}=\frac{2}{j\rho^{(i)}}\int_{-\infty}^{\infty}S^{(i)}dc_y \qquad \tau^{(i)}=\frac{3\tau_{tr}^{(i)}+j\tau_{rot}^{(i)}}{3+j} \quad (20)$$

$$q_{tr}^{(i)}=\int_{-\infty}^{\infty}\left(c_y^2F^{(i)}+G^{(i)}\right)c_ydc_y \qquad q_{rot}^{(i)}=\int_{-\infty}^{\infty}S^{(i)}c_ydc_y \qquad q^{(i)}=q_{tr}^{(i)}+q_{rot}^{(i)} \quad (21)$$

It is noted that the conservation equation $\partial q^{(i)}(y)/\partial y = 0$, $i = H, R, A$ is readily deduced, which implies that the total heat flux $q^{(i)}(y)$ remains constant along $-1/2 \le y \le 1/2$. The Rykov model at its present form is applicable only to diatomic gases ($j = 2$), while the Holway model is applicable to polyatomic gases ($j = 2, 3$).

3.2 The ES-BGK model for polyatomic gases

The ES-BGK model for polyatomic gases proposed by Andries et al. [30], has received less attention since it has been proposed more recently. Its applicability is demonstrated in [41] where some typical rarefied gas flows are solved and a comparison with corresponding results based on the Boltzmann equation is provided. In terms of the reduced distribution functions the model, for the present heat transfer problem is written as [30,41]

$$c_y \frac{\partial \boldsymbol{\Psi}^{(A)}}{\partial y} = \delta_0 \rho^{(A)} \left(\tau_{tr}^{(A)}\right)^{1-\omega} \left(\frac{1}{1-\nu+\theta\nu}\right)\left[\boldsymbol{\Psi}_{eq}^{(A)} - \boldsymbol{\Psi}^{(A)}\right] \tag{22}$$

where the superscript (A) denotes the Andries model and $\boldsymbol{\Psi}^{(A)} = \left[F^{(A)}, G^{(A)}, S^{(A)}, R^{(A)}\right]^T$ is the vector of the unknown reduced distributions. In this model the reduced equilibrium functions in Eq. (22) are kept in compact form $\boldsymbol{\Psi}_{eq}^{(A)} = \left[F_{eq}^{(A)}, G_{eq}^{(A)}, S_{eq}^{(A)}, R_{eq}^{(A)}\right]^T$, where

$$F_{eq}^{(A)} = \frac{\rho^{(A)}}{\sqrt{\pi K_{yy}}} \exp\left[-c_y^2 K_{yy}^{-1}\right] \qquad G_{eq}^{(A)} = \frac{\rho^{(A)}\left(K_{xx}+K_{zz}\right)}{2\sqrt{\pi K_{yy}}} \exp\left[-c_y^2 K_{yy}^{-1}\right],$$

$$S_{eq}^{(A)} = \frac{j\rho^{(A)}\tau_{rel}^{(A)}}{2\sqrt{\pi K_{yy}}} \exp\left[-c_y^2 K_{yy}^{-1}\right] \qquad R_{eq}^{(A)} = \frac{\rho^{(A)} K_{xx}}{2\sqrt{\pi K_{yy}}} \exp\left[-c_y^2 K_{yy}^{-1}\right] \tag{23}$$

with the tensor $\boldsymbol{K}_{ii}$, $i = x, y, z$, written as

$$\boldsymbol{K}_{ii} = (1-\theta)\left[(1-\nu)\tau_{tr}^{(A)} + 2\nu\frac{P_{ii}^{(A)}}{\rho^{(A)}}\right] + \theta\tau^{(A)}. \tag{24}$$

The quantity $\tau_{rel}^{(A)}$ in Eq. (23) is a new "artificial" temperature, which is accordingly decomposed as

$$\tau_{rel}^{(A)} = \theta\tau^{(A)} + (1-\theta)\tau_{rot}^{(A)}. \tag{25}$$

where $\tau^{(A)}$ and $\tau_{rot}^{(A)}$ are the total and rotational temperatures respectively. The relaxation parameters $-1/2 \le \nu < 1$ and $0 \le \theta \le 1$ are chosen to recover the correct Prandtl number of diatomic and polyatomic gases according to

$$\frac{2}{3} \le \Pr = \frac{1}{1-\nu+\theta\nu} < \infty \tag{26}$$

For a monatomic gas a Prandtl of 2/3 is obtained by taking $\theta = 0$ and $\nu = -1/2$. In that case the ES model kinetic model for monatomic gases is recovered.

The macroscopic quantities of number density $\rho^{(A)}$, translational, rotational and total temperatures $\tau_{tr}^{(A)}$, $\tau_{rot}^{(A)}$ and $\tau^{(A)}$ respectively as well as the corresponding heat fluxes $q_{tr}^{(A)}$, $q_{rot}^{(A)}$ and $q^{(A)}$ are given by Eqs. (19-21), with $i = A$, while the normal stresses in Eq. (24) are

$$P_{xx}^{(A)} = \int_{-\infty}^{\infty} R^{(A)} dc_y \quad P_{yy}^{(A)} = \int_{-\infty}^{\infty} F^{(A)} c_y^2 dc_y \quad P_{zz}^{(A)} = \int_{-\infty}^{\infty} \left(G^{(A)} - R^{(A)} \right) dc_y \tag{25}$$

It is noted that the entropy inequality (H-theorem) has been proved for this polyatomic kinetic model with $-1/2 \le \nu < 1$ and $0 < \theta < 1$ in [30].

3.3 Boundary conditions

To close the problem the formulation of the boundary conditions at $y = \pm 1/2$ for the reflected distributions is provided. The classical Maxwell wall model is applied [42]. Hereby, to distinguish between incident and reflected quantities the superscripts $(+)$ and $(-)$ are introduced.

At the boundaries the thermal accommodation coefficients for the translational and rotational energy are respectively defined as [18,23]

$$\alpha_{tr} = \frac{E_{tr}^{-} - E_{tr}^{+}}{E_{tr}^{-} - E_{tr}^{w}} \qquad \alpha_{rot} = \frac{E_{rot}^{-} - E_{rot}^{+}}{E_{rot}^{-} - E_{rot}^{w}} \tag{26}$$

where E_{tr}^{-} and E_{rot}^{-} are the incident translational and rotational energy fluxes, $E_{tr}^{+} = 2Nk_B T_{tr}^{\alpha}$ and $E_{rot}^{+} = (j/2) Nk_B T_{rot}^{\alpha}$ are the reflected translational and rotational energy fluxes, while $E_{tr}^{w} = 2Nk_B T^{w}$ and $E_{rot}^{w} = (j/2) Nk_B T^{w}$ are the translational and rotational energy fluxes that would have been achieved if the reflected molecules were emitted in thermal equilibrium at the surface. The incident and reflected particle fluxes are equal to each other and they are both

denoted by $N=-\int_{\xi_y<0}\int_0^\infty \xi_y f dI d\boldsymbol{\xi}$, T^w is the surface temperature, while T_{tr}^α and T_{rot}^α are parameters to be obtained as part of the solution from the energy balances, i.e. Eqs. (26), at the surface. The thermal accommodation coefficients vary between unity (complete accommodation, diffuse reflection) and zero (adiabatic, specular reflection).

The distribution function of the polyatomic particles reflected from the surfaces has the following form [34]:

$$f^+ = n_w\left[\frac{m}{2\pi k_B T_{tr}^\alpha}\right]^{3/2}\exp\left[-\frac{m\boldsymbol{\xi}^2}{2k_B T_{tr}^\alpha}\right]\frac{\hat{I}^{j/2-1}}{\left(k_B T_{rot}^\alpha\right)^{j/2}\Gamma\left(j/2\right)}\exp\left[-\frac{\hat{I}}{k_B T_{rot}^\alpha}\right] \tag{27}$$

Introducing in Eq. (27), the same normalization and projection process as for the kinetic equations, lead to the following reflected reduced distributions at the boundaries $y=\pm 1/2$:

$$F^+ = \frac{\rho_w}{\sqrt{\pi\tau_{tr}^\alpha}}\exp\left[-c_y^2/\tau_{tr}^\alpha\right] \qquad G^+ = \tau_{tr}^\alpha F^+ \qquad S^+ = \frac{j}{2}\tau_{rot}^\alpha F^+ \qquad R_i^+ = \frac{1}{2}\tau_{tr}^\alpha F^+ \tag{28}$$

The parameter ρ_w is computed as

$$\rho_{w,i} = \frac{2\sqrt{\pi}}{\sqrt{\tau^\alpha}}\int_0^\infty F^- c_y dc_y \tag{29}$$

from the condition that the walls are not permeable to the gas. The parameters $\tau_{tr}^\alpha = T_{tr}^\alpha / T_0$ and $\tau_{rot}^\alpha = T_{rot}^\alpha / T_0$ are calculated from the energy balance equations for the rotational and translational degrees of freedom at the surface according to

$$\tau_{tr}^\alpha = \alpha_{tr}\tau + (1-\alpha_{tr})\frac{E_{tr}^-}{2N} \qquad \tau_{rot}^\alpha = \alpha_{rot}\tau + (1-\alpha_{rot})\frac{2E_{rot}^-}{jN} \tag{30}$$

with

$$\frac{E_{tr}^-}{N} = \frac{\int_0^\infty\left(c_y^2 F^- + G^-\right)c_y dc_y}{\int_0^\infty F^- c_y dc_y} \qquad \frac{E_{rot}^-}{N} = \frac{\int_0^\infty S^- c_y dc_y}{\int_0^\infty F^- c_y dc_y}. \tag{31}$$

The boundary conditions (28-31), with the two thermal accommodation coefficients, separate contributions from the different energy modes and provide a detailed description of the energy transfer between the gas and the surface.

However in most occasions, experimental studies report only one energy accommodation coefficient defined as

$$\alpha = \frac{E^- - E^+}{E^- - E^w}. \tag{32}$$

Now, the energy fluxes in Eq. (32) are obtained by adding the corresponding translational and rotational parts, i.e. $E^- = E_{tr}^- + E_{rot}^-$, $E^+ = \left(2 + j/2\right) N k_B T^\alpha$ and $E^w = \left(2 + j/2\right) N k_B T^w$, while $T^\alpha = T_{tr}^\alpha = T_{rot}^\alpha$. The reflected reduced distributions are given by

$$F^+ = \frac{\rho_w}{\sqrt{\pi \tau^\alpha}} \exp\left[-c_y^2 / \tau^\alpha\right] \qquad G^+ = \tau^\alpha F^+ \qquad S^+ = \frac{j}{2} \tau^\alpha F^+ \qquad R^+ = \frac{1}{2} \tau^\alpha F^+ \tag{33}$$

where $\tau_{rot}^\alpha = \tau_{tr}^\alpha = \tau^\alpha$ and

$$\tau^\alpha = \alpha \tau + (1 - \alpha) \frac{2E^-}{\left(4 + j\right) N} \tag{34}$$

while

$$\frac{E^-}{N} = \frac{\int_0^\infty \left(c_y^2 F^- + G^- + S^-\right) c_y dc_y}{\int_0^\infty F_i^- c_y dc_y}. \tag{35}$$

This approach with the one thermal accommodation coefficient is simpler and modeling remains efficient.

Furthermore, to take into account the cross energy transfer between the translational and rotational modes two additional energy accommodations may be introduced into the two thermal accommodation coefficients model resulting to a total of four coefficients [18]. Thus, a better adjustment to experimental results is allowed but since the number of parameters to be examined is increased this type of boundary conditions seems to be more useful in investigations focused on specific comparisons between simulations and experiments.

In the present work the kinetic model equations of Holway, Rykov and Andries with the associated moments applying both types of boundary conditions described above are solved numerically in a deterministic manner. The discretization is based on the discrete velocity method in the molecular velocity space and on a second order control volume approach in the physical space. The macroscopic quantities are computed by Gauss-Legendre quadrature. The implemented algorithm is parallel in the velocity space and has been extensively applied in previous works to solve with considerable success heat transfer configurations [3,29]. The iteration process between the kinetic equations and the corresponding moments of the distribution functions is terminated when the convergence criteria

$$\frac{1}{3K}\sum_{i=1}^{K}\left[\left|\rho_i^{(t+1)}-\rho_i^{(t)}\right|+\left|\tau_i^{(t+1)}-\tau_i^{(t)}\right|+\left|q_i^{(t+1)}-q_i^{(t)}\right|\right]<\varepsilon \tag{36}$$

with t denoting the iteration index and K the number of nodes in the physical space, is fulfilled. The kinetic results presented here have been obtained with 4001 equally spaced nodes and 96 molecular velocities being the roots of the corresponding Legendre polynomial, while the tolerance parameter is set to $\varepsilon=10^{-8}$.

Computations have been performed with a parallel version of the code parallelizing in the molecular velocity space on 3 Intel(R) Core(TM) i5-3570 cpus at 3.40GHz (total of 12 cores). The computational times per iteration for the BGK, Shakhov, Holway, Andries and Rykov models are roughly speaking in the ratio 1:2:3:4:6, i.e. the computational time of the polyatomic models is approximately three times higher than the corresponding monatomic ones. It is noted that the total number of iterations for convergence depends only on the reference rarefaction parameter and is independent of the model. To have an idea of the required computational times, it is stated indicatively that the simulation of the case $\delta_0=50$, $T_H/T_C=3$ with the above defined parallelization and numerical parameters, based on the Holway model, takes about 3.2min (*serial* execution time about 32min).

The computational results always coincide in the free molecular limit ($\delta_0=0$) with the corresponding analytical results of the translational and rotational temperatures and heat fluxes. Also, as δ_0 is increased, the computed heat flux gradually tends to the analytical one in the hydrodynamic limit. The analytical solutions in the two limits are provided in the Appendix B.

4. DSMC solution of the Boltzmann equation

In order to assess the capabilities of the kinetic model described in previous sections, the problem has also been studied by solving the Boltzmann equation for a gas of linear rigid rotators. When, as in the case considered here, intrinsic molecular angular momenta (spin) have no preferential alignment, it is desirable to describe molecular internal states through a single variable, the internal energy I or the angular momentum modulus. Then, the gas is described by a spin orientation averaged distribution function $f(\hat{\boldsymbol{r}},\boldsymbol{v},I,t)$ which obeys a Boltzmann equation in the usual general form [17]:

$$\frac{\partial f}{\partial t}+\boldsymbol{v}\frac{\partial f}{\partial \hat{\boldsymbol{r}}}=Q(f,f), \tag{37}$$

However, the presence of internal states in the collision dynamics and cross section makes the structure of the collision integral Q more complicated than in the monatomic gas case [17]. The determination of the form of the collision cross section is not easy. As is well known, the dynamics of a binary *molecular* collision is much more complicated than a binary *atomic* collision which is largely amenable to analytical treatment. Simple mechanical models of translational-rotational coupling (rough spheres, loaded spheres, spherocylinders) [43] are not flexible enough to fit experimental data on polyatomic species.

Hence, the collision dynamics and cross-sections have been obtained from the well-known phenomenological model proposed by Borgnakke and Larsen (B-L) [31]. The model has strong similarities with Holway's kinetic model. Actually, it describes the coupling between translational and internal degrees of freedom by mixing elastic and inelastic collisions. In inelastic molecular encounters, post-collisional values of internal states are obtained sampling an equilibrium probability density. However, the overall binary collision probability more realistically depends on relative velocity, according to the adopted total collision cross section model. This is not the case for the kinetic models considered in this work, whose collision frequency does not depend on molecular velocity.

In spite of its phenomenological nature, B-L model parameters can be easily adapted to reproduce experimental translational-rotational relaxation rates with good accuracy [44]. Further validation of B-L model is provided by the results of more sophisticated and computationally demanding CT-DSMC simulations in which molecular collisions are accurately computed by Classical Trajectories [45], on the basis of potential energy surfaces (PES's), obtained by molecular beams scattering experiments [46] or *ab initio* quantum chemistry methods. Figure 1 compares B-L density and temperature profiles in molecular Oxygen, confined between two parallel plates, to similar computations based on Classical Trajectories modeling of O_2-O_2 encounters [46]. The wall temperatures T_C and T_H have been set respectively equal to $400\,\mathrm{K}$ and $600\,\mathrm{K}$. The reference Knudsen number computed from O_2 viscosity at $\left(T_C + T_H\right)/2$ is equal to $1/35$. The B-L implementation has been based on hard sphere cross section and a temperature independent rotational relaxation number $Z^{(DSMC)} = 5$. Full accommodation at walls has been assumed for both B-L and CT-DSMC simulations. As the comparison shows, B-L model provides a very good approximation of the accurate collision dynamics provided by Classical Trajectories simulations, for the considered heat transfer geometry.

In order to provide comparisons with kinetic models predictions, steady, spatially one-dimensional solutions of Eq. (37) have been obtained as the long time limit of unsteady solutions, numerically computed by a DSMC scheme [47] in which $f\left(\hat{y},\boldsymbol{v},I,t\right)$ is represented by a large number of mathematical particles. Each of them is characterized by velocity $\boldsymbol{v}\left(t\right)$, rotational energy $I(t)$ and spatial position $\hat{y}(t)$, being $\hat{y}$ the coordinate which spans the gap between the plates. As is well known, the particles states are advanced from time t to time $t+\Delta t$ in two stages. In the first stage gas-gas collisions are neglected and particles move along straight lines with the constant velocity and rotational energy they had at time t. In this free flight stage wall boundary conditions are applied to change the velocity and internal energy of molecules hitting a wall. In the second stage, particles positions are kept fixed and equal to the final values resulting from the free flight. Particles belonging to the same cell of the spatial grid are allowed to collide according to the rule described above. In all DSMC simulations, a diatomic gas has been considered ($j=2$). Hard spheres collision cross section has been assumed in combination with a standard implementation of B-L model [29], in which a temperature independent value of the parameter $Z^{(DSMC)}$ has been used. Macroscopic quantities are obtained by sampling and time averaging particles microscopic states after the onset of steady flow conditions.

Gas-surface interaction is described by Maxwell's model which allows velocities of molecules hitting a solid wall to be diffusively scattered with probability α or specularly reflected with probability $1-\alpha$. When specular reflection occurs, the internal energy I is not changed by the collision with a wall. In the case of diffuse scattering, internal energy is sampled from the wall Maxwellian given by Eq. (27). The reported DSMC results have been obtained from simulations using not less than 1250 particles per cell. The spatial cell size $\Delta\hat{y}$ does not exceed $1/20$ of the reference mean free path. The time step Δt has been set equal to the minimum between the estimated time a particle takes to cross a cell, $\left(\Delta t\right)_{adv}=\Delta\hat{y}/\sqrt{RT_H}$, and a small fraction $\left(\Delta t\right)_{col}$ of the minimum mean free time, based on the maximum value ν_c of the collision frequency in the domain. Macroscopic quantities have been obtained by sampling microscopic particles states for $20-40\times10^4$ time steps after the estimated onset of steady conditions. The heat fluxes data in Table 4 and the distributions of density and temperature in Figs. 2 and 3 have been obtained by averaging samples of ten statistically independent

simulations for each temperature and rarefaction parameter setting. The heat fluxes dispersion within each sample allows estimating the statistical error associated with the Monte Carlo method. In most of the cases the relative statistical error is well below 1%. Larger relative standard deviations (around 2%) are found for the largest value of the rarefaction parameter and the smallest temperature ratio.

The computing time associated to a *serial* DSMC simulation amounts to about 1.3×10^{-7} s per time step, per particle, on a workstation equipped with Intel Xeon E5-2630 cpus, running at 2.3 Ghz. For instance, the simulation of the case $\delta_0 = 50$, $T_H / T_C = 3$ with 1000 spatial cells and 2.0×10^5 particles, takes about 40min to execute 3.0×10^5 time steps and produce an accurate solution. The performances of a parallel version of the code can be estimated by considering that well designed DSMC parallel implementations have an efficiency close to 80% [48].

5. Results and discussion

Results for the heat fluxes and the distributions of temperature and density obtained by the Holway, Rykov and Andries models as well as by the DSMC method in a wide range of all involved parameters are presented in tabulated and graphical form. The temperature ratio of the hot over the cold plate takes the values of $T_H / T_C = (1+\beta)/(1-\beta) = [1.1, 3, 7, 10]$ covering the cases of small, moderate and large temperature differences, while the reference gas rarefaction parameter $\delta_0 \in [0, 100]$ varies in a wide range of the gas rarefaction from the free molecular up to the slip regime. Two types of gas-surface interaction are considered and comparisons with measurements under various conditions are included.

The results are organized as follows: Section 5.1 presents results of the heat fluxes for diatomic and polyatomic gases as well as a comparison between kinetic and DSMC results including density and temperature fields. Section 5.2 describes the dependency of the heat fluxes on the accommodation coefficients and finally, Section 5.3 is focused on comparison with experiments.

5.1 Heat fluxes and comparison between kinetic and DSMC results

In Tables 1 and 2 the dimensionless translational and rotational heat fluxes respectively obtained by all three kinetic models are compared for a diatomic gas ($j = 2$, $\mathrm{Pr} = 0.72$) with HS molecules. The temperature ratio and the reference gas rarefaction parameter take the values of

$T_H / T_C = [1.1, 3, 10]$ and $\delta_0 \in [0, 100]$ respectively. Since the translational and rotational heat fluxes vary between the plates the tabulated results are at the hot plate ($y = -1/2$). Of course the total heat flux remains constant. The gas molecules are fully accommodated at the two plates. Furthermore, in order to ensure comparison compatibility between the various kinetic models and according to the Appendix A (Eq. (A4)), where the relaxation rates are discussed, the rotational collision numbers are set as $Z^{(R)} = Z^{(A)} = 6.50$ and $Z^{(H)} = Z^{(A)} \times \Pr = 4.67$. Based on these values and $\kappa = 1/1.2$ (HS molecules) it is deduced that $\varpi_o = 0.458$, $\varpi_1 = 2.840$ in the Rykov model and $\nu = -0.50$, $\theta = 0.21$ in the Andries model. It is clearly seen that for both heat fluxes the agreement between the corresponding results obtained by all three models is excellent (within two or even three significant figures for all values of δ_0 and T_H / T_C). The rotational heat flux is always about one-half of the corresponding translational one, while in the free molecular limit, is exactly one-half. The results for $\delta_0 = 0$ coincide with the corresponding analytical ones estimated by Eqs. (B3) in Appendix B.

It is noted that the dependency of the results on the values of $Z^{(i)}$ for the present heat transfer configuration and for all values of δ_0 and T_H / T_C tested, in all three models, is small, with the Holway model being the less sensitive one. Also, as $Z^{(i)}$ is increased the translational heat flux tends to the heat flux of a monatomic gas, while the rotational heat flux remains always about one-half of the translational one. To clearly demonstrate that, in Table 3, the monatomic heat fluxes obtained by the BGK and Shakhov model are tabulated for the same temperature ratios T_H / T_C and rarefaction gas parameters δ_0 [49]. It is seen that the monoatomic heat fluxes are close to and always a little bit higher than the translational part of the corresponding diatomic heat flux, shown in Table 1, while the total diatomic heat fluxes $q^{(i)} = q_{tr}^{(i)} + q_{rot}^{(i)}$ are higher compared to the corresponding monatomic ones of Table 3 about 30-50 %.

A comparison between the dimensionless total heat fluxes obtained by the Andries model and the DSMC method for a diatomic gas with $Z^{(DSMC)} = Z^{(A)} = 5$ ($\nu = -0.5$, $\theta = 0.27$) is presented in Table 4. The particles reflection is purely diffuse at the walls. The temperature ratio and the reference gas rarefaction parameter take the values of $T_H / T_C = [1.1, 3, 7, 10]$ and $\delta_0 \in [0, 100]$ respectively. In all cases the agreement between the results is very good with the relative error being less than 3%. Furthermore, the comparison is extended to the number density distributions

plotted in Fig. 2 as well as to the translational and rotational temperature distributions plotted in Fig. 3 for various typical values of δ_0 and T_H / T_C demonstrating excellent agreement between the deterministic and stochastic approaches. It is also seen that the translational and rotational distributions are very close to each other and through Eq. (11) it is deduced that $\tau \simeq \tau_{tr} \simeq \tau_{rot}$, with the larger deviations occurring at larger temperature differences and intermediate values of the gas rarefaction. Overall, the effectiveness of the Andries as well as of the Holway and Rykov models to simulate this heat transfer configuration is clearly demonstrated.

In Table 5 the translational and rotational heat fluxes of a polyatomic gas ($j = 3$) based on the Andries model with $Z^{(A)} = 6.50$, $\nu = -0.50$, $\theta = 0.21$ and purely diffuse reflection at the walls are tabulated. The results are at the hot plate for $T_H / T_C = [1.1, 3, 7, 10]$ and $\delta_0 \in [0,100]$. Overall, the qualitative variation of the polyatomic heat fluxes in terms of T_H / T_C and δ_0 is similar to the diatomic ones. More specifically, the translational parts of the polyatomic and diatomic heat fluxes are close, while the rotational part of the polyatomic heat flux is always higher than the corresponding one of the diatomic gas. Comparing the total polyatomic heat fluxes with those in Table 3, it is deduced that they are about 50-75% higher than the corresponding monatomic ones. The analytical free molecular solutions are fully recovered with the rotational part to be 75% of the translational one.

5.2 Effect of accommodation coefficients

The effect of partial accommodation at the walls on the heat fluxes is investigated based on the two types of boundary conditions presented in Section 3.3. Results are provided for the typical values $T_H / T_C = [1.1, 3, 10]$, $\delta_0 \in [0,100]$ and they are based on the Holway kinetic model.

First the boundary condition (33-35) with the one energy accommodation coefficient $\alpha \in [0,1]$, defined by Eq. (32), is considered. In Fig. 4, the dimensionless total heat flux $q^{(H)}$ of a diatomic gas ($j = 2$, $\mathrm{Pr} = 0.71$, $Z^{(H)} = 5$) with HS molecules in terms of α is plotted. As expected the effect of α on the total heat flux becomes more significant as δ_0 is decreased, i.e. as the gas becomes more rarefied, while at $\delta_0 = 100$ the total heat flux is practically independent of α. Also, in almost all cases as α is increased the dimensionless total heat flux is monotonically increased, which is physically justified since a larger portion of particles are

reflected with temperatures closer to the wall temperatures. However, for large temperature differences this is true only at large δ_0, while as δ_0 is decreased a maximum heat flux is observed at some $\alpha < 1$. This is clearly shown at $T_H / T_C = 10$ and $\delta_0 \le 0.1$, where the maximum heat flux is reached at about $\alpha = 0.95$. It has been found that as the temperature ratio is further increased the value of α where the maximum heat flux occurs is decreased. The behavior of both the translational and rotational parts of the heat flux with respect to α is similar to the one described here for the total heat flux and therefore is not shown separately. These findings have also been confirmed by simulations with the other kinetic models and the DSMC approach. In addition, the results for $\delta_0 = 0$ are in excellent agreement with the corresponding analytical ones given in the Appendix B, where the detailed dependence of q_{fm} on the parameters α and β is shown in Fig. 12.

Next, the boundary condition (28-31) with the two energy accommodation coefficients $\alpha_{tr} \in [0,1]$ and $\alpha_{rot} \in [0,1]$, defined by Eqs. (26), is considered and the effect of the accommodation coefficients on each of the translational and rotational parts of the heat flux is investigated. In Fig. 5, the dimensionless translational heat flux $q_{tr}^{(H)}$ at the hot plate of a diatomic gas ($j = 2$, $\mathrm{Pr} = 0.71$, $Z = 5$) with HS molecules in terms of α_{tr} with $\alpha_{rot} = 1$ as well as in terms of α_{rot} with $\alpha_{tr} = 1$ is plotted. It is seen that the dependency of $q_{tr}^{(H)}$ on α_{tr} is very similar to the one observed before of $q^{(H)}$ on α. On the contrary $q_{tr}^{(H)}$ is actually independent of α_{rot}.

In Fig. 6, the corresponding plots for $q_{rot}^{(H)}$ are provided. The rotational heat flux depends on both α_{tr} and α_{rot}. With regard to α_{tr} the dependency is in general weak in small temperature differences but becomes stronger as the temperature difference is increased and the gas becomes more rarefied. It is interesting to observe that in these latter conditions as α_{tr} is increased $q_{rot}^{(H)}$ is decreased. With regard to α_{rot} the dependency of the rotational heat flux is strong and as α_{rot} is increased, $q_{rot}^{(H)}$ is also increased.

The effect of the two thermal accommodation coefficients on the density and temperature distributions is shown in Figs. 7 and 8 for a diatomic HS gas ($j = 2$, $\mathrm{Pr} = 0.71$, $Z = 5$) in the case of $T_H / T_C = 10$ and $\delta_0 = 1$. The dimensionless wall temperatures are $\tau_H = 1.82$ and $\tau_C = 0.18$.

More specifically, in Fig. 7 the distributions of density and translational temperature are plotted for various values of α_{tr} with $\alpha_{rot}=1$. It is seen that at small values of α_{tr} both distributions, even at this large temperature ratio, are almost anti-symmetric about $y=0$ (typical of a linear configuration) and then as α_{tr} is increased the anti-symmetry is vanished (typical of a nonlinear configuration). The effect of the variation of α_{tr} on the wall temperature jump is more dominant at the cold rather than in the hot wall. The coefficient α_{rot} has always a very small effect or no effect at all on these distributions and therefore its effect is not plotted. On the contrary, both α_{tr} and α_{rot} have an important effect on the rotational temperature shown in Fig. 8. It is seen that as α_{tr} is increased, $\tau_{rot}^{(H)}(y)$ is decreased in a uniform manner along the distance y (the curves are almost parallel to each other). Also, at large values of α_{rot}, the $\tau_{rot}^{(H)}(y)$ distribution is antisymmetric and as α_{rot} is decreased it becomes antisymmetric. In addition, as T_H/T_C is decreased the effect of α_{tr} and α_{rot} on $\tau_{rot}^{(H)}(y)$ is drastically decreased.

Furthermore, comparing the translational and rotational temperatures in Figs. 7 and 8 respectively with $\alpha_{tr}\le 1$ and $\alpha_{rot}=1$ it is seen that $\tau_{tr}^{(H)}\simeq\tau_{rot}^{(H)}$ only when $\alpha_{tr}=1$ while as α_{tr} is reduced the translational and rotational temperatures start to depart of each other. To clearly demonstrate that the two temperatures are plotted for $\alpha_{tr}=1$, $\alpha_{rot}=0.2$ and $\alpha_{tr}=0.2$, $\alpha_{rot}=1$ at two different values of the reference gas rarefaction parameter in Fig. 9. It is seen that for $\alpha_{tr}\neq\alpha_{rot}$, i.e., when translational and rotational energies are differently accommodated at the walls, then the corresponding temperatures vary significantly ($\tau_{tr}^{(H)}\neq\tau_{rot}^{(H)}$) and this difference becomes larger as δ_0 is decreased. Also, at $\delta_0=0.1$ the departure between $\tau_{tr}^{(H)}$ and $\tau_{rot}^{(H)}$ is larger with the variation of α_{rot} rather than of α_{tr}. It is expected that similar results will be obtained performing molecular dynamics simulations.

5.3 Comparison with experiments

A comparison with the early experimental results in [27] and the more recent ones in [13] is performed based on the kinetic Holway model and the DSMC method. In both experiments the temperature difference between the plates is small, the gas is nitrogen (N_2) and the associated energy accommodation coefficient have been experimentally determined from heat transfer

measurements at low pressures where the Knudsen formula is valid to be about $\alpha = 0.75 - 0.8$. The simulations have been performed for a diatomic HS gas with $\mathrm{Pr} = 0.71$ with the experimental accommodation coefficients, while the rotational collision number for the DSMC approach is taken to be $Z^{(DSMC)} = 5$.

The comparison with [27] is shown in Fig. 10 in terms of the total heat flux normalized with the corresponding free molecular heat flux versus the inverse of the reference Knudsen number. The measured temperature of the hot plate and the temperature ratio are $T_H = 301.96\,\mathrm{K}$ and $T_H / T_C = 1.0291$ respectively, while the experimentally determined thermal accommodation coefficient is $\alpha = 0.76$. The Holway model simulations have been performed for these data with $Z^{(H)} = 5$ as well as with Z obtained by the Landau-Teller (L-T) expression [47] based on the Lordi and Mates [50] experimental data. As it is seen the computed results are in very good agreement with the experimental ones in the whole range of the inverse Knudsen number. It is noted however, that the implemented gas-surface interaction model is not capable to capture both the heat flux and density variations presented in [27] simultaneously and to achieve that more complex boundary conditions, as the ones in [18] are needed.

The comparison with [13] is shown in Fig. 11 in terms of the dimensionless total heat flux q versus the inverse measured pressure. The measured temperatures of the hot and cold plates are $T_H = 308.3$ K and $T_C = 288.3$ K respectively ($T_H / T_C = 1.069$), while the associated experimentally estimated thermal accommodation coefficients are $\alpha_H = 0.795$ and $\alpha_C = 0.808$ [13]. Simulations have been performed for these data with the Holway model ($Z^{(H)} = 5$). Excellent agreement between the kinetic results and measurements is observed in the whole range of measured pressures.

In order to obtain a more physical understanding of the heat transfer in monatomic and polyatomic gases and to facilitate comparisons with experiments, in Fig. 12, some dimensional total heat fluxes [W/m^2] in terms of the reference pressure P_0 [Pa] are given for the monatomic gases of He and Ar ($j = 0$, $\mathrm{Pr} = 0.67$), the diatomic gases of H_2 and N_2 ($j = 2$, $\mathrm{Pr} = 0.71$) and for the polyatomic gas of CO_2 ($j = 3$, $\mathrm{Pr} = 0.75$). The distance between the plates is $H = 5\,\mathrm{mm}$ with the temperature of the cold plate to be set at $T_C = 293\,\mathrm{K}$ and temperature ratio $T_H / T_C = 3$. The reference pressure $P_0 \in \left[10^{-4}, 10^{2}\right]$ Pa is easily connected to the rarefaction parameter δ_0, via

Eq. (8) once the viscosity and the most probable velocity of each gas is specified. All computations are based on the Holway model and the VHS interaction law with $\omega = [0.66, 0.81, 0.67, 0.74, 0.93, 0.84]$ for He, Ar, H_2, N_2, CO_2, CH_4 respectively. It is noted that the experimentally estimated rotational collision number of these gases may vary between one and five [39]. However, the dependency of the results on Z is small and therefore in all cases $Z^{(H)} = 5$ is introduced. It is seen that, as expected, the heat flux is monotonically increased with pressure. At highly rarefied atmospheres the heat flux is proportional to gas pressure, then, in the transition regime the relation becomes more complex and at dense atmospheres the heat flux depends weakly and finally is independent of pressure.

More importantly, it is observed in Fig. 12, that under the same conditions the heat flux of different gases varies significantly. The largest heat fluxes are achieved for H_2 followed successively by the heat fluxes of He, CH_4, N_2, CO_2 and Ar. This trend is valid in the whole range of pressure except for the curves of CO_2 and Ar, which cross each other at some relatively large pressure $P_0 > 1$ Pa. In monatomic gases confined between surfaces the heat transfer is increased as the molar mass of the gas is decreased and the molecular velocities are increased. However, this remark cannot be generalized in the case of polyatomic gases since the additional degrees of freedom result to additional heat transfer, as seen in Fig. 12, where in a wide range of pressure the heat flux of CO_2 is larger than that of Ar, while its molar mass is larger.

6. Concluding remarks

The problem of heat transfer through rarefied polyatomic gases confined between two parallel plates maintained at different temperatures is solved based on three kinetic models namely the ones proposed by Holway, Rykov and Andries as well as on the DSMC scheme supplemented by the Borgnakke-Larsen collision model. Results for the heat fluxes and the distributions of density and temperature are provided for small, moderate and large temperature differences in a wide range of the gas rarefaction from the free molecular limit up to the slip regime with full and partial energy accommodation at the boundaries. The three kinetic models and the DSMC method provide very close values of the computed macroscopic quantities as well as very good agreement with corresponding experimental data available in the literature. In addition, the computational results perfectly match the analytical ones in the free molecular limit and tend to the analytical ones in the hydrodynamic regime.

Based on the above, the validity of the implemented modeling approaches is demonstrated. All kinetic models provide accurate results for the specific problem. The H-theorem has been proved for the Andries model and can be readily obtained for the Holway model, while no such proof exists for the Rykov model. Surely, the Holway model is the simplest to use since it depends only on one parameter, the Prandtl number, but probably not accurate enough to treat problems with combined heat transfer and flow phenomena. The Rykov model remains a solid alternative for diatomic gases, while very recently has been extended to polyatomic gases [51]. It is noted that for this specific heat transfer problem the dependency of the results on the parameter indicating the strength of translational-rotational coupling is very small for all kinetic models and the DSMC method (the Holway model is the less sensitive one).

The total heat fluxes of diatomic and polyatomic gases have been found to be higher about 30–50% and 50–75% respectively than the corresponding monatomic ones, with the highest differences occurring in the free molecular limit. Furthermore, as the amount of elastic compared to inelastic collisions is increased, the translational heat fluxes are slightly increased and they tend to the monatomic ones, while always the rotational heat fluxes are about 50% and 75% of the translational ones for diatomic and polyatomic gases respectively. Also, the translational and rotational temperature distributions (as well as the total temperature) are very close to each other for each set of parameters examined and they are similar to the corresponding monatomic ones when the translational and rotational accommodation coefficients are the same. On the contrary they depart from each other when the two coefficients are different. In most cases as the thermal accommodation coefficient α is increased, i.e. the gas-surface interaction becomes more diffusive, the dimensionless total heat flux is monotonically increased. However, for adequately large temperature differences and efficiently high gas rarefaction levels a non-monotonic behavior, with a maximum total heat flux at some $\alpha < 1$ has been observed. A detailed description of the behavior of the translational and rotational heat fluxes and temperatures on the partial energy accommodation at the walls is provided. Finally, providing some dimensional results, it has been found that while in monatomic gases the heat flux is always increased as the molar mass is decreased, this is not necessarily the case in polyatomic gases since the additional degrees of freedom result to additional heat transfer.

Overall, it is noted that the present work may be useful in the heat transfer design and optimization of MEMS, vacuum sensors and other technological devices with polyatomic gases. It is also noted that the presented results are in a range of heat transfer parameters where the

assumption of a gas of rigid rotators is justified, while future work will refer to polyatomic gases taking into consideration the vibrational degrees of freedom.

Acknowledgments

This project has received funding from the European Union's Horizon 2020 research and innovation programme under grant agreement number 633053. The views and opinions expressed herein do not necessarily reflect those of the European Commission.

Appendix A: Relaxation rates in a homogenous gas

Comparisons between the translational-rotational relaxation rates of the applied kinetic model equations and those of the DSMC method with the Borgnakke-Larsen collision model are performed. Consider a homogeneous polyatomic gas at a constant equilibrium total temperature with different initial rotational and translational temperatures. Then, the rotational and translational temperatures will evolve and relax into the constant equilibrium total temperature with rates related to the collision frequencies. By operating accordingly on the kinetic model equations the time evolution of the translational-rotational temperatures may be obtained. Then, the parameter $Z^{(i)}$ is accordingly fixed to ensure equivalent translational and rotational relaxation rates in order to have a consistent comparison.

The kinetic model equations (14) and (22) are rewritten for a time-dependent homogeneous system, i.e., by adding the time derivative term and omitting all space derivatives terms. Then, they are accordingly combined and the resulting equations are integrated over the velocity space to yield the following relaxation equations for each model:

- Holway:

$$\frac{\partial \tau_{tr}^{(H)}}{\partial t} = \frac{8}{5\sqrt{\pi}} \Pr \frac{\sqrt{\tau_{tr}^{(H)}}}{Z^{(H)}} \left[\tau^{(H)} - \tau_{tr}^{(H)} \right] \qquad \frac{\partial \tau_{rot}^{(H)}}{\partial t} = \frac{8}{5\sqrt{\pi}} \Pr \frac{\sqrt{\tau_{tr}^{(H)}}}{Z^{(H)}} \left[\tau^{(H)} - \tau_{rot}^{(H)} \right] \tag{A1}$$

- Rykov:

$$\frac{\partial \tau_{tr}^{(R)}}{\partial t} = \frac{8}{5\sqrt{\pi}} \frac{\sqrt{\tau_{tr}^{(R)}}}{Z^{(R)}} \left[\tau^{(R)} - \tau_{tr}^{(R)} \right] \qquad \frac{\partial \tau_{rot}^{(H)}}{\partial t} = \frac{8}{5\sqrt{\pi}} \frac{\sqrt{\tau_{tr}^{(R)}}}{Z^{(R)}} \left[\tau^{(R)} - \tau_{rot}^{(R)} \right] \tag{A2}$$

- Andries:

$$\frac{\partial \tau_{tr}^{(A)}}{\partial t} = \frac{8}{5\sqrt{\pi}} \frac{\sqrt{\tau_{tr}^{(A)}}}{Z^{(A)}} \left[\tau^{(A)} - \tau_{tr}^{(A)} \right] \qquad \frac{\partial \tau_{rot}^{(A)}}{\partial t} = \frac{8}{5\sqrt{\pi}} \frac{\sqrt{\tau_{tr}^{(A)}}}{Z^{(A)}} \left[\tau^{(A)} - \tau_{rot}^{(A)} \right] \tag{A3}$$

All above equations have been deduced by introducing hard-sphere interactions ($\omega = 1/2$) and the dimensionless time $t = \tilde{t} / \left(\lambda_0 / \upsilon_0 \right)$, with $\lambda_0 = 1/\left(\sqrt{2} \pi d^2 n_0 \right)$ and d denoting the molecular diameter, as well as the equation $\partial n / \partial t = 0$. It is also noted that in the relaxation equations of the Andries model $Z^{(A)} = \left(1 - \nu + \theta \nu \right) / \theta$ and $\mathrm{Pr} = \left(1 - \nu + \theta \nu \right)^{-1}$.

The relaxation rates of the kinetic model equations have been compared numerically with the corresponding ones of the DSMC method. It has been found that by setting

$$Z^{(DSMC)} = Z^{(A)}\left(\nu, \theta \right) = Z^{(R)}\left(\varpi_0, \varpi_1 \right) = \frac{Z^{(H)}}{\mathrm{Pr}} \tag{A4}$$

where $Z^{(DSMC)}$ denotes the rotation collision parameter in the DSMC simulations, nearly identical translational-rotational relaxation rates are produced in all cases. The relations between the rotational collision numbers of the three kinetic models, shown in Eq. (A4), are well justified by Eqs. (A1-A3), while their connection to $Z^{(DSMC)}$ is validated numerically. Some indicative results are demonstrated in Fig. 13, where the time evolution of the translational and rotational temperatures towards the equilibrium temperature for a diatomic gas with $\mathrm{Pr} = 0.73$ and initial conditions $\tau_{tr}^{(i)}\left(0 \right) = 3$ and $\tau_{rot}^{(i)}\left(0 \right) = 1$, are shown. It is seen that for $Z^{(DSMC)} = Z^{(R)} = Z^{(A)} = 5$ and $Z^{(H)} = 3.65$ excellent agreement in the relaxation towards equilibrium between all models is obtained. The rotational collision number $Z^{(A)}$ has been obtained with $\nu = -0.5$ and $\theta = 0.273$, while $Z^{(H)} = Z^{(DSMC)}\,\mathrm{Pr}$. On the contrary for $Z^{(H)} = 5$ the Holway model presents a slower relaxation towards equilibrium. Equation (A4) is used in Section 5.1 to define the rotational collision number for the various kinetic models and the DSMC method in order to have a consistent comparison between the computed heat fluxes.

Appendix B: Analytical solutions at the free molecular and hydrodynamic limits

In the free molecular limit ($\delta_0 = 0$) the right hand side of the kinetic model equations (14) and (22) becomes zero and then based on the associated boundary conditions closed form expressions for the reduced distributions functions $\boldsymbol{\Psi}^{(i)}$ are readily deduced, which are substituted into the moment equations (19-21) and (25) to yield analytical results for the macroscopic distributions. It is noted that in the free molecular limit all moments are independent of y and remain constant at any position between the plates. Following this procedure and using boundary conditions (33) and (34), the translational and rotational heat

fluxes in terms of the thermal accommodation coefficient α and the normalized temperature difference β are given by

$$q_{tr,fm}(\alpha,\beta)=\frac{1}{\sqrt{\pi}}\left[\left(1+\frac{1}{\gamma}\right)^{3/2}\left(1-\gamma+\sqrt{\gamma^2-1}\right)-\left(1-\frac{1}{\gamma}\right)^{3/2}\left(1+\gamma-\sqrt{\gamma^2-1}\right)\right] \tag{B1}$$

and

$$q_{rot,fm}(\alpha,\beta)=\frac{j}{4}q_{tr,fm}(\alpha,\beta) \tag{B2}$$

respectively, where $\gamma=(2-\alpha)/(\alpha\beta)$. For the specific case of purely diffuse reflection ($\alpha=1$ and $\gamma=1/\beta$), Eqs. (B1) and (B2) are reduced to

$$q_{tr,fm}(\beta)=\frac{2}{\sqrt{\pi}}\left[(1+\beta)\sqrt{1-\beta}-(1-\beta)\sqrt{1+\beta}\right] \quad \text{and} \quad q_{rot,fm}(\beta)=\frac{j}{4}q_{tr,fm}(\beta). \tag{B3}$$

In Fig. 14 the free molecular total heat flux $q_{fm}=q_{tr,fm}+q_{tr,fm}$ is plotted for a diatomic gas ($j=2$) in terms of the parameters α and β. It is seen that at small β, q_{fm} is monotonically increased with the thermal accommodation coefficient α and the maximum q_{fm} occurs at $\alpha=1$. However, at large β the corresponding behavior is non-monotonic and the maximum q_{fm} appears at some value of $\alpha<1$. Similar results have also been obtained in Section 5.2 for $\delta_0>0$, provided that the temperature difference is adequately large and the gas rarefaction parameter remains low.

In the hydrodynamic limit ($\delta_0\to\infty$) the Fourier law is introduced into the energy equation to yield the total heat flux. Following the same procedure as in [29], where the Eucken correction is introduced, it is readily deduced that for a HS gas

$$q(\delta_0\to\infty)=\left(\frac{5}{4}+\frac{j}{6}\right)\frac{\left[(1+\beta)^{3/2}-(1-\beta)^{3/2}\right]}{\delta_0}. \tag{B4}$$

The tabulated numerical results in Section 5.1 for $j=0,2,3$ tend to the corresponding analytical results of Eq. (B4) at large values of the gas rarefaction parameter.

References

1. J. L. Strapasson, F. Sharipov, Ab initio simulation of heat transfer through a mixture of rarefied gases, International Journal of Heat and Mass Transfer, 71, 91-97, 2014.
2. M. Vargas, S. Stefanov, V. Roussinov, Transient heat transfer flow through a binary gaseous mixture confined between coaxial cylinders, International Journal of Heat and Mass Transfer, 59, 302-315, 2013.
3. S. Pantazis, D. Valougeorgis, Non-linear heat transfer through rarefied gases between coaxial cylindrical surfaces at different temperatures, European Journal of Mechanics B/Fluids, 29, 494-509, 2010.
4. I. Graur, A. P. Polikarpov, Comparison of different kinetic models for the heat transfer problem, Heat Mass Transfer, 46 (2), 237-244, 2009.
5. W. Jitschin, S. Ludwig, Dynamical behavior of the Pirani sensor, Vacuum, 75, 169-176, 2004.
6. S. J. O'shea, R. E. Collins, An experimental study of conduction heat transfer in rarefied polyatomic gases, International Journal of Heat and Mass Transfer, 35 (12), 3431-3440, 1992.
7. P. J. Sun, J. Y. Wu, P. Zhang, L. Xu, M. L. Jiang, Experimental study of the influences of degraded vacuum on multilayer insulation blankets, Cryogenics, 49, 719-726, 2009.
8. Y. Yang, I. Gerken, J. J. Brandner, G. L. Morini, Design and experimental investigation of a gas-to-gas counter-flow micro heat exchanger, Experimental Heat Transfer, 27 (4), 340-359, 2014.
9. H. Chalabi, O. Buchina, L. Saraceno, M. Lorenzini, D. Valougeorgis, G. L. Morini, Experimental analysis of heat transfer between a heated wire and a rarefied gas in an annular gap with high diameter ratio, Journal of Physics: Conference Series, 362, 012028, 2012.
10. S. C. Saxena, Trasport properties of gases and gaseous mixtures at high temperatures, High temperature science, 3, 168-188, 1971.
11. F. Sharipov and D. Kalempa, Velocity slip and temperature jump coefficients for gaseous mixtures. IV. Temperature jump coefficient, International Journal of Heat and Mass Transfer, 48 (6), 1076-1083, 2005.
12. Y. G. Semyonov, S. F. Borisov, P. E. Suetin, Investigation of heat transfer in rarefied gases over a wide range of Knudsen number, International Journal of Heat and Mass Transfer, 27 (10), 1789-1799, 1984.
13. W. M. Trott, J. N. Castaneda, J. R. Torczynski, M. A. Gallis, D. J. Rader, An experimental assembly for precise measurement of thermal accommodation, Review of Scientific Instruments, 82, 0355120, 2011.
14. H. Yamaguchi, K. Kanazawa, Y. Matsuda, T. Niimi, A. Polikarpov, I. Graur, Investigation on heat transfer between two coaxial cylinders for measurement of thermal accommodation coefficient, Physics of Fluids, 24, 062002, 2012.
15. J. H. Ferziger, H. G. Kaper, Mathematical Theory of Transport Processes in Gases, North-Holland Publishing Company, Amsterdam, 1972.
16. G. A. Bird, Monte Carlo simulation of gas flows, Annual Review of Fluid Mechanics, 10, 11-31, 1978.
17. I. Kuscer, A model for rotational energy exchange in polyatomic gases, Physica A, 158, 784-800, 1989.
18. I. N. Larina, V. A. Rykov, Boundary conditions for gases on a body surface, Fluid Dynamics, 21, 795 – 801, 1986.
19. T. F. Morse, Kinetic model for gases with internal degrees of freedom, Physics of Fluids, 7 (2), 159-169, 1964.
20. L. H. Holway, New statistical models for kinetic theory: Methods of construction, Physics of Fluids, 9 (9), 1658-1672, 1966.
21. F. B. Hanson, T. F. Morse, Kinetic models for a gas with internal structure, Physics of Fluids, 10 (2), 345-353, 1967.
22. S. K. Hsu, T. F. Morse, Kinetic theory of parallel heat transfer in a polyatomic gas, Physics of Fluids, 15 (4), 584-591, 1972.

23. P. Pazooki, S. K. Loyalka, Heat transfer in a polyatomic gas – I. Plane parallel plates, International Journal of Heat and Mass Transfer, 28 (11), 2019-2027, 1985.
24. B. Huang, P. F. Hwang, Test of statistical models for gases with and without internal energy states, Physics of Fluids, 16 (4), 466-475, 1973.
25. V. A. Rykov, A model kinetic equation for a gas with rotational degrees of freedom, Fluid Dynamics, 10 (6), 956-966, 1975.
26. I. N. Larina, V. A. Rykov, Kinetic model of the Boltzmann equation for a diatomic gas with rotational degrees of freedom, Computational Mathematics and Mathematical Physics, 50, 2118-2130, 2010.
27. W. P. Teagan, G. S. Springer, Heat transfer and density-distribution measurements between parallel plates in the transition regime, Physics of Fluids, 11 (3), 497-506, 1968.
28. D. J. Alofs, R. C. Flagan, G. S. Springer, Density distribution measurements in rarefied gases contained between parallel plates at high temperature differences, Physics of Fluids, 14 (3), 529-533, 1971.
29. C. Tantos, D. Valougeorgis, M. Pannuzzo, A. Frezzotti, G. L. Morini, Conductive heat transfer in a rarefied polyatomic gas confined between coaxial cylinders, International Journal of Heat Mass Transfer, 79, 378-389, 2014.
30. P. Andries, P. L. Tallec, J. P. Perlat, B. Perthame, The Gaussian-BGK model of Boltzmann equation with small Prandtl number, European Journal of Mechanics B/Fluids, 19, 813-830, 2000.
31. C. Borgnakke, P. S. Larsen, Statistical collision model for Monte Carlo simulation of polyatomic gas mixture, Journal of Computational Physics, 18 (4), 405-420, 1975.
32. P. L. Bhatnagar, E. P. Gross, M. A. Krook, A model for collision processes in gases. I. Small amplitude processes in charged and neutral one-component systems, Phys. Review, 94, 511-525, 1954.
33. E. M. Shakhov, Generalization of the Krook kinetic relaxation equation, Fluid Dynamics, 3 (5), 95-95, 1968.
34. A. Frezzotti, A numerical investigation of the steady evaporation of a polyatomic gas, European Journal of Mechanics B/Fluids, 26, 93-104, 2007.
35. V. A. Titarev, E. M. Shakhov, Poiseuille flow and thermal creep in a capillary tube on the basis of the R-Model, Fluid Dynamics, 47, 661-672, 2012.
36. S. Liu, P. Yu, K. Xu, C. Zhong, Unified gas-kinetic schemes for diatomic molecular simulations in all flow regimes, Journal of Computational Physics, 259, 96-113, 2014.
37. J. Jean, An Introduction to the Kinetic Theory of Gases, Cambridge University Press, (page 216), 1967.
38. J. O. Hirschfelder, C. F. Curtiss, R. B. Bird, Molecular Theory of Gases and Liquids, Wiley, New York, 1954.
39. E. A. Mason, L. Monchick, Heat conductivity of polyatomic and polar gases, The Journal of Chemical Physics, 36 (6), 1622-1639, 1962.
40. V. A. Rykov, V. N. Skobelkin, Macroscopic description of the motions of a gas with rotational degrees of freedom, Mekhanika Zhidkosti i Gaza, No. 1, 180-183, 1978.
41. P. Andries, J. F. Bourgan, P. Tallec, B. Perthame, Numerical comparison between the Boltzmann and ES-BGK models for rarefied gases, Computer methods in Applied Mechanics and Engineering, 191, 3369-3390, 2002.
42. J. C. Maxwell, The Scientific Papers of James Clerk Maxwell, Volume 2, Cambridge University Press, London, 1890.
43. S. Chapman, T. G. Cowling, The Mathematical Theory of Non-Uniform Gases, Cambridge University Press, Cambridge UK, 1990.
44. I. J. Wysong, D. C. Wadsworth, Assessment of direct simulation Monte Carlo phenomenological rotational relaxation models, Physics of Fluids, 10, 2983-2994, 1998.
45. D. Bruno, A. Frezzotti, G. P. Ghiroldi, Oxygen transport properties estimation by DSMC-CT simulations, Proceedings of the 29th International Symposium on Rarefied Gas-Dynamics, AIP Conference Proceedings, Vol. 1628, 108 , 2014.

46. V. Aquilanti, D. Ascenzi, M. Bartolomei, D. Cappelletti, S. Cavalli, M. de Castro Vitores, F. Pirani, Molecular beam scattering of aligned oxygen molecules. The nature of the bond in the O_2-O_2 dimer, Journal of American Chemical Society, 121, 10794-10802, 1999.
47. G. A. Bird, Molecular Gas Dynamics and the Direct Simulation of Gas Flows, Clarendon Press, Oxford, 1994.
48. J. S. Wu and K. C. Tseng, Parallel DSMC method using dynamic domain decomposition, International Journal for Numerical methods in Engineering, 63, 37-76, 2005.
49. S. Pantazis, D. Valougeorgis, Heat transfer between parallel plates via kinetic theory in the whole range of the Knudsen number, Paper 407, 5th European Thermal-Sciences Conference, 19-22/5/2008, Eindhoven, Netherlands, 2008.
50. J. A. Lordi, R. E. Mates, Rotational Relaxation in nonpolar diatomic gases, Physics of Fluids, 13 (2), 291-308, 1970.
51. L. Wu, C. White, T. J. Scanlon, J. M. Reese and Y. Zhang, A kinetic model of the Boltzmann equation for non-vibrating polyatomic gases, Journal of Fluid Mechanics, 763, 24-50, 2015.

Table 1: Dimensionless translational heat fluxes $q_{tr}^{(i)}$, $i = A, H, R$ for a diatomic gas ($j = 2$, $\mathrm{Pr} = 0.72$) with HS molecules ($\omega = 0.5$) at the hot plate ($y = -1/2$) and various values of δ_0 and T_H / T_C ($Z^{(R)} = Z^{(A)} = 6.50$, $\nu = -0.50$, $\theta = 0.21$, $\varpi_o = 0.458$, $\varpi_1 = 2.840$, $Z^{(H)} = 4.67$).

δ_0	$T_H / T_C = (1+\beta)/(1-\beta)$								
	1.1			3.0			10.0		
	Andries	Holway	Rykov	Andries	Holway	Rykov	Andries	Holway	Rykov
0	5.37(-2)	5.37(-2)	5.37(-2)	5.06(-1)	5.06(-1)	5.06(-1)	5.98(-1)	5.98(-1)	5.98(-1)
0.1	5.11(-2)	5.11(-2)	5.09(-2)	4.84(-1)	4.84(-1)	4.83(-1)	5.83(-1)	5.83(-1)	5.88(-1)
1	3.79(-2)	3.79(-2)	3.77(-2)	3.65(-1)	3.65(-1)	3.66(-1)	4.68(-1)	4.67(-1)	4.82(-1)
5	1.92(-2)	1.92(-2)	1.95(-2)	1.92(-1)	1.92(-1)	1.95(-1)	2.75(-1)	2.75(-1)	2.85(-1)
10	1.21(-2)	1.21(-2)	1.23(-2)	1.22(-1)	1.22(-1)	1.25(-1)	1.84(-1)	1.84(-1)	1.90(-1)
50	3.03(-3)	3.03(-3)	3.10(-3)	3.13(-2)	3.13(-2)	3.20(-2)	4.96(-2)	4.96(-2)	5.07(-2)
100	1.56(-3)	1.57(-3)	1.60(-3)	1.62(-2)	1.62(-2)	1.66(-2)	2.58(-2)	2.58(-2)	2.64(-2)

Table 2: Dimensionless rotational heat fluxes $q_{rot}^{(i)}$, $i = A, H, R$ for a diatomic gas ($j = 2$, $\mathrm{Pr} = 0.72$) with HS molecules ($\omega = 0.5$) at the hot plate ($y = -1/2$) and various values of δ_0 and T_H / T_C ($Z^{(R)} = Z^{(A)} = 6.50$, $\nu = -0.50$, $\theta = 0.21$, $\varpi_o = 0.458$, $\varpi_1 = 2.840$, $Z^{(H)} = 4.67$).

δ_0	$T_H / T_C = (1+\beta)/(1-\beta)$								
	1.1			3.0			10.0		
	Andries	Holway	Rykov	Andries	Holway	Rykov	Andries	Holway	Rykov
0	2.68(-2)	2.68(-2)	2.68(-2)	2.53(-1)	2.53(-1)	2.53(-1)	2.99(-1)	2.99(-1)	2.99(-1)
0.1	2.54(-2)	2.54(-2)	2.51(-2)	2.40(-1)	2.40(-1)	2.39(-1)	2.90(-1)	2.90(-1)	2.91(-1)
1	1.80(-2)	1.80(-2)	1.74(-2)	1.74(-1)	1.74(-1)	1.69(-1)	2.24(-1)	2.24(-1)	2.24(-1)
5	8.55(-3)	8.55(-3)	8.11(-3)	8.59(-2)	8.59(-2)	8.20(-2)	1.25(-1)	1.24(-1)	1.21(-1)
10	5.27(-3)	5.27(-3)	4.98(-3)	5.39(-2)	5.38(-2)	5.12(-2)	8.18(-2)	8.18(-2)	7.85(-2)
50	1.31(-3)	1.31(-3)	1.25(-3)	1.36(-2)	1.36(-2)	1.29(-2)	2.17(-2)	2.16(-2)	2.05(-2)
100	6.79(-4)	6.79(-4)	6.44(-4)	7.05(-3)	7.04(-3)	6.68(-3)	1.12(-2)	1.12(-2)	1.07(-2)

Table 3: Dimensionless heat flux for a monatomic gas with HS molecules ($\omega = 0.5$) for various values of δ_0 and T_H / T_C based on the BGK and Shakhov models.

δ_0	$T_H / T_C = (1+\beta)/(1-\beta)$					
	1.1		3.0		10.0	
	BGK	Shakhov	BGK	Shakhov	BGK	Shakhov
0	5.37(-2)	5.37(-2)	5.06(-1)	5.06(-1)	5.98(-1)	5.98(-1)
0.1	5.13(-2)	5.09(-2)	4.86(-1)	4.84(-1)	5.85(-1)	5.89(-1)
1	3.86(-2)	3.81(-2)	3.72(-1)	3.70(-1)	4.74(-1)	4.88(-1)
5	2.02(-2)	2.01(-2)	2.01(-1)	2.02(-1)	2.86(-1)	2.94(-1)
10	1.28(-2)	1.28(-2)	1.30(-1)	1.31(-1)	1.95(-1)	1.98(-1)
50	3.31(-3)	3.31(-3)	3.43(-2)	3.43(-2)	5.42(-2)	5.43(-2)
100	1.72(-3)	1.72(-3)	1.78(-2)	1.78(-2)	2.84(-2)	2.84(-2)

Table 4: Comparison between the dimensionless total heat fluxes q of the Andries model and the DSMC method for a diatomic gas ($j = 2$, $\mathrm{Pr} = 0.73$) with HS molecules ($\omega = 0.5$) and various values of δ_0 and T_H / T_C ($Z^{(DSMC)} = Z^{(A)} = 5$, $\nu = -0.5$, $\theta = 0.27$).

δ_0	$T_H / T_C = (1+\beta)/(1-\beta)$							
	1.1		3.0		7.0		10.0	
	Andries	DSMC	Andries	DSMC	Andries	DSMC	Andries	DSMC
0.1	7.64(-2)	7.55(-2)	7.24(-1)	7.21(-1)	8.90(-1)	8.87(-1)	8.73(-1)	8.70(-1)
1	5.56(-2)	5.57(-2)	5.36(-1)	5.35(-1)	6.86(-1)	6.81(-1)	6.89(-1)	6.81(-1)
5	2.74(-2)	2.80(-2)	2.74(-1)	2.80(-1)	3.77(-1)	3.82(-1)	3.95(-1)	3.99(-1)
10	1.71(-2)	1.75(-2)	1.73(-1)	1.78(-1)	2.46(-1)	2.52(-1)	2.62(-1)	2.68(-1)
50	4.26(-3)	4.38(-3)	4.41(-2)	4.55(-2)	6.47(-2)	6.68(-2)	6.99(-2)	7.23(-2)
100	2.20(-3)	2.28(-3)	2.28(-2)	2.38(-2)	3.36(-2)	3.50(-2)	3.63(-2)	3.78(-2)

Table 5: Dimensionless translational and rotational heat fluxes for a polyatomic gas ($j = 3$, $\mathrm{Pr} = 0.72$) with HS molecules ($\omega = 0.5$) at the hot plate ($y = -1/2$) and various values of δ_0 and T_H / T_C based on the Andries model ($Z^{(A)} = 6.50$, $\nu = -0.50$, $\theta = 0.21$).

δ_0	$T_H / T_C = (1+\beta)/(1-\beta)$							
	1.1		3.0		7.0		10.0	
	$q_{tr}^{(A)}$	$q_{rot}^{(A)}$	$q_{tr}^{(A)}$	$q_{rot}^{(A)}$	$q_{tr}^{(A)}$	$q_{rot}^{(A)}$	$q_{tr}^{(A)}$	$q_{rot}^{(A)}$
0	5.37(-2)	4.03(-2)	5.06(-1)	3.79(-1)	6.14(-1)	4.61(-1)	5.98(-1)	4.49(-1)
0.1	5.11(-2)	3.80(-2)	4.84(-1)	3.61(-1)	5.95(-1)	4.43(-1)	5.83(-1)	4.35(-1)
1	3.79(-2)	2.70(-2)	3.65(-1)	2.61(-1)	4.66(-1)	3.34(-1)	4.68(-1)	3.36(-1)
5	1.92(-2)	1.28(-2)	1.91(-1)	1.29(-1)	2.62(-1)	1.78(-1)	2.75(-1)	1.86(-1)
10	1.20(-2)	7.88(-3)	1.22(-1)	8.05(-2)	1.73(-1)	1.15(-1)	1.83(-1)	1.22(-1)
50	3.01(-3)	1.96(-3)	3.11(-2)	2.03(-2)	4.57(-2)	2.98(-2)	4.93(-2)	3.23(-2)
100	1.56(-3)	1.01(-3)	1.61(-2)	1.05(-2)	2.37(-2)	1.55(-2)	2.57(-2)	1.67(-2)

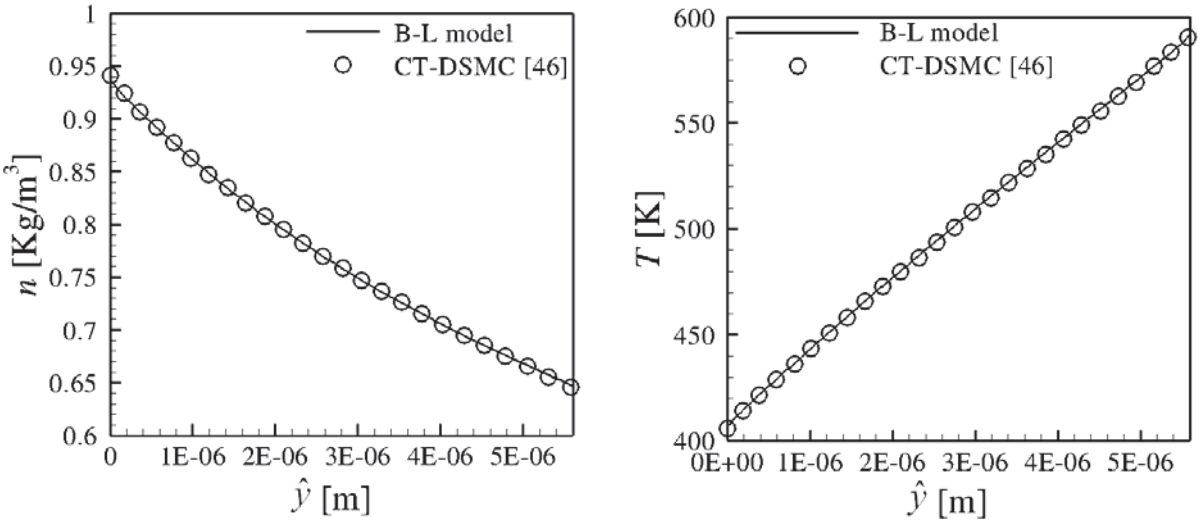

Figure 1: Comparison of B-L model and CT-DSMC [45] predictions of density (left) and temperature (right) fields in gaseous O_2 confined between parallel plates with $T_C = 400$ K, $T_H = 600$ K and reference Knudsen number equal to 1/35.

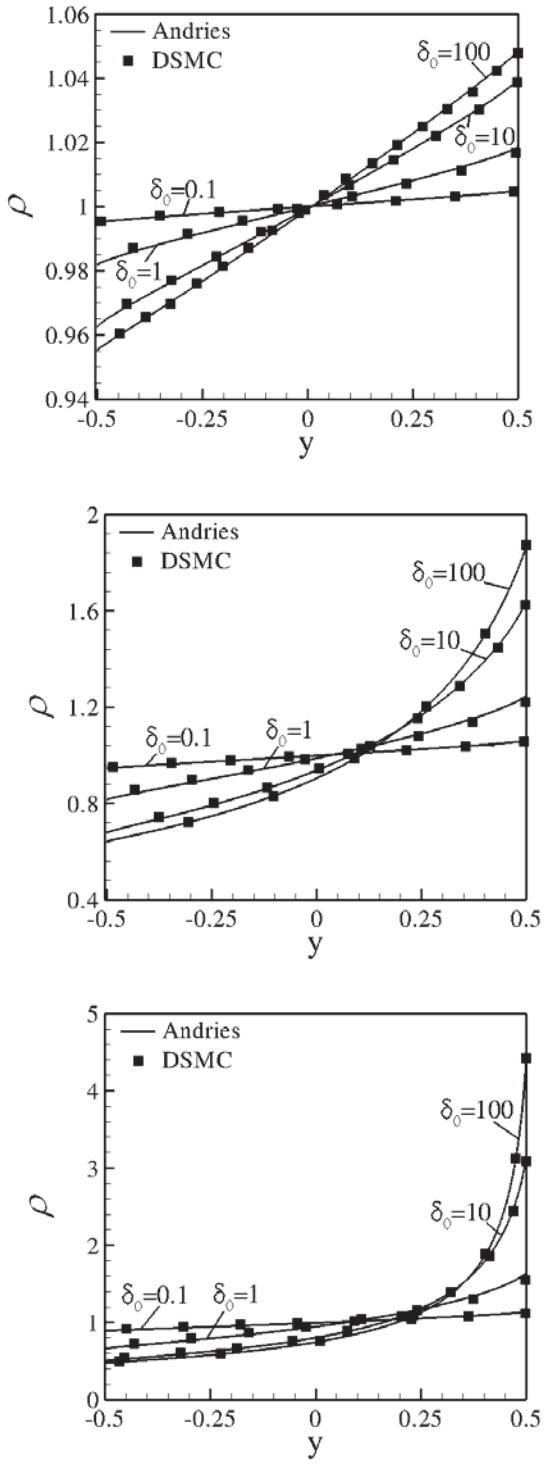

Figure 2: Comparison between the dimensionless number density distributions $\rho(y)$ of the Andries model and the DSMC method for a diatomic HS gas ($j=2$, $\Pr=0.73$, $Z^{(DSMC)}=Z^{(A)}=5$, $\nu=-0.5$, $\theta=0.27$) and various values of δ_0 with $T_H/T_C=1.1$ (up), $T_H/T_C=3$ (middle) and $T_H/T_C=10$ (down).

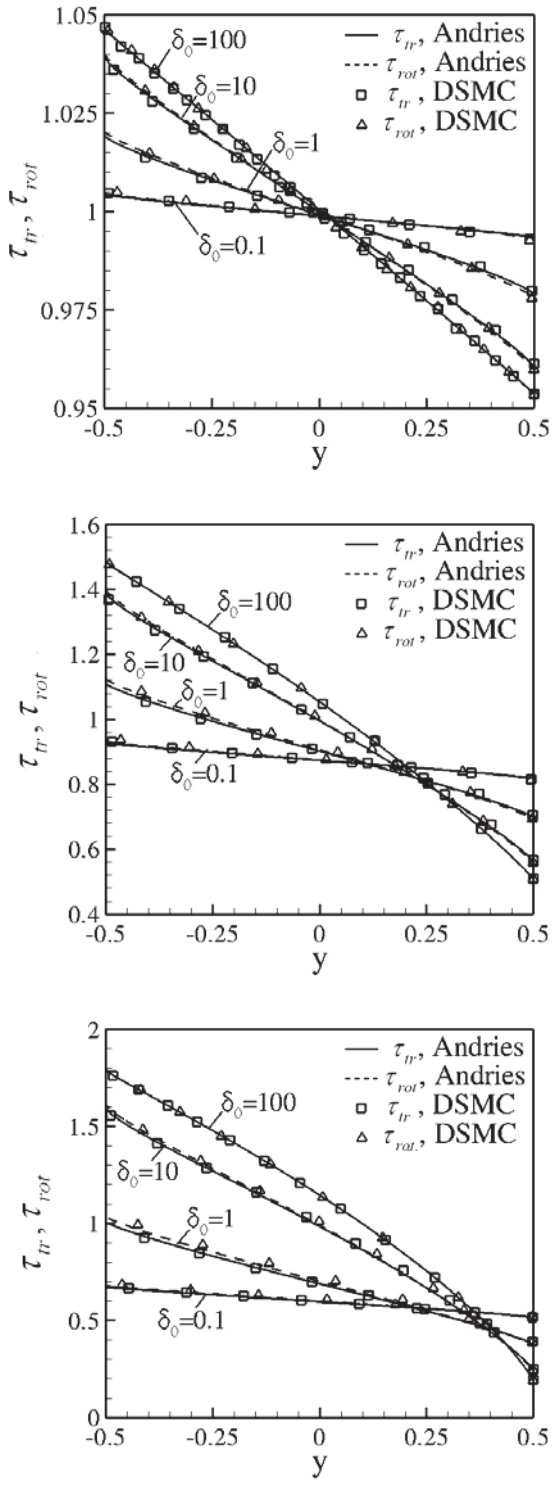

Figure 3: Comparison between the dimensionless translational $\tau_{tr}(y)$ and rotational $\tau_{rot}(y)$ temperature distributions of the Andries model and the DSMC method for a diatomic HS gas ($j=2$, $\mathrm{Pr}=0.73$, $Z^{(DSMC)}=Z^{(A)}=5$, $\nu=-0.5$, $\theta=0.27$) and various values of δ_0 with $T_H/T_C=1.1$ (up), $T_H/T_C=3$ (middle) and $T_H/T_C=10$ (down).

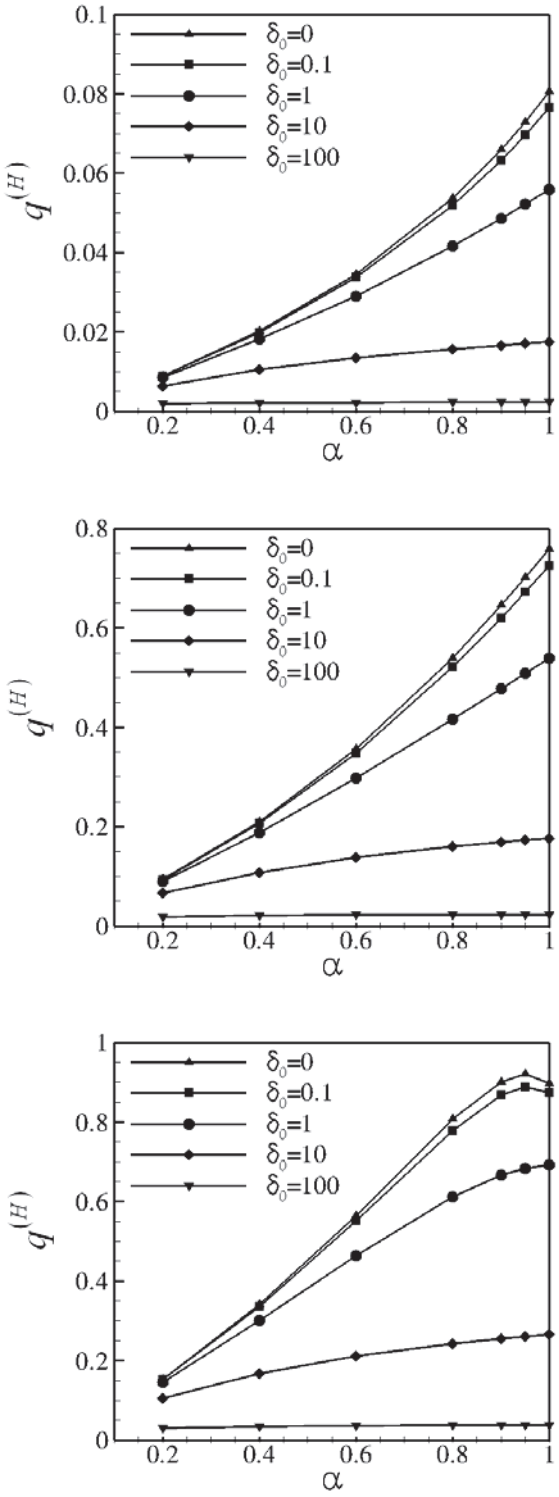

Figure 4: Dimensionless total heat flux $q^{(H)}$ of a diatomic HS gas ($j=2$, $\mathrm{Pr}=0.71$, $Z^{(H)}=5$) in terms of thermal accommodation coefficient α for various values of δ_0 and $T_H/T_C=1.1$ (up), $T_H/T_C=3$ (middle), $T_H/T_C=10$ (down) based on the Holway model.

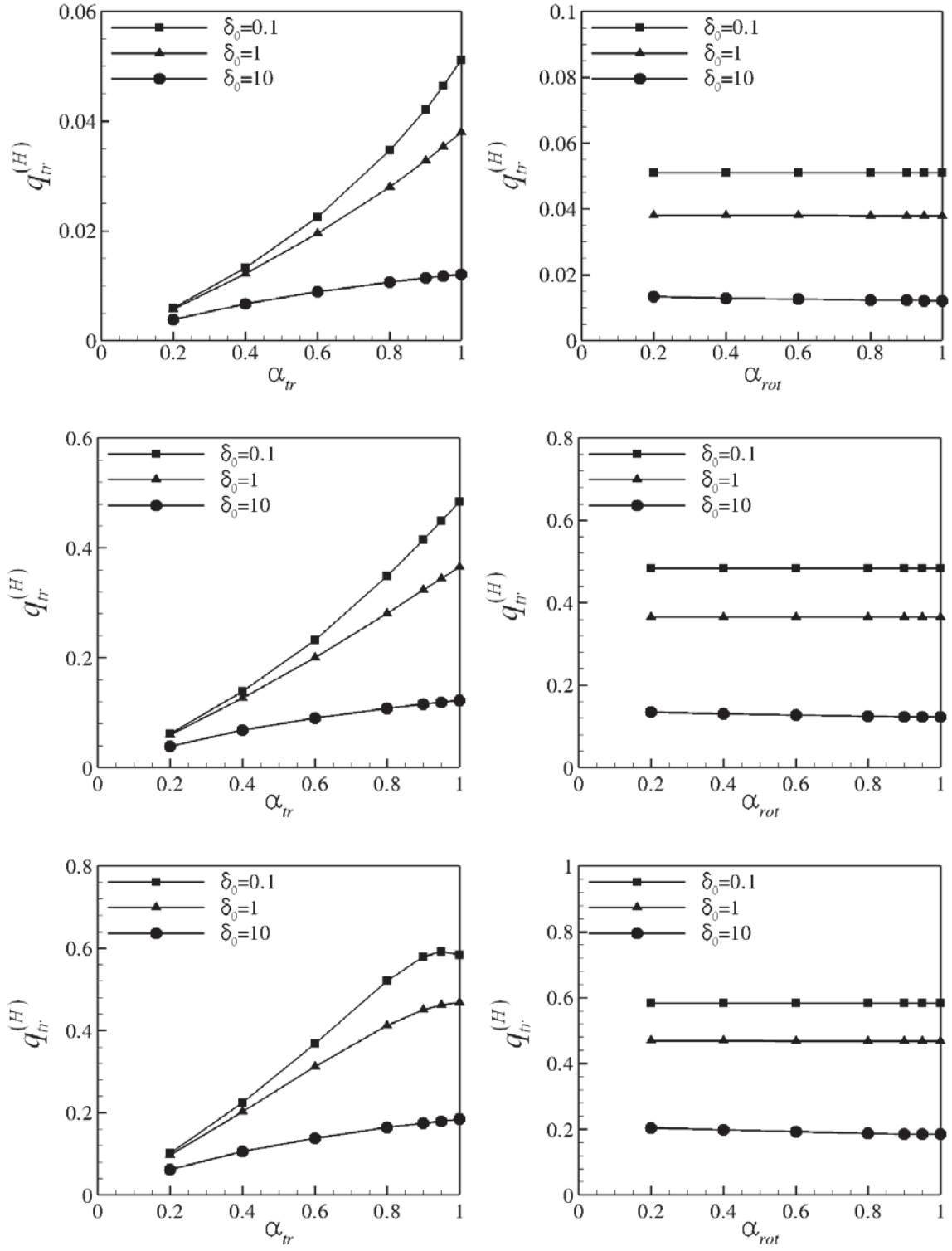

Figure 5: Dimensionless translational heat flux $q_{tr}^{(H)}$ at the hot plate of a diatomic HS gas ($j=2$, $\mathrm{Pr}=0.71$, $Z=5$) in terms of α_{tr} (left) and α_{rot} (right) for $\delta_0=[0.1,1,10]$ and $T_H/T_C=1.1$ (up), $T_H/T_C=3$ (middle), $T_H/T_C=10$ (down) based on the Holway model.

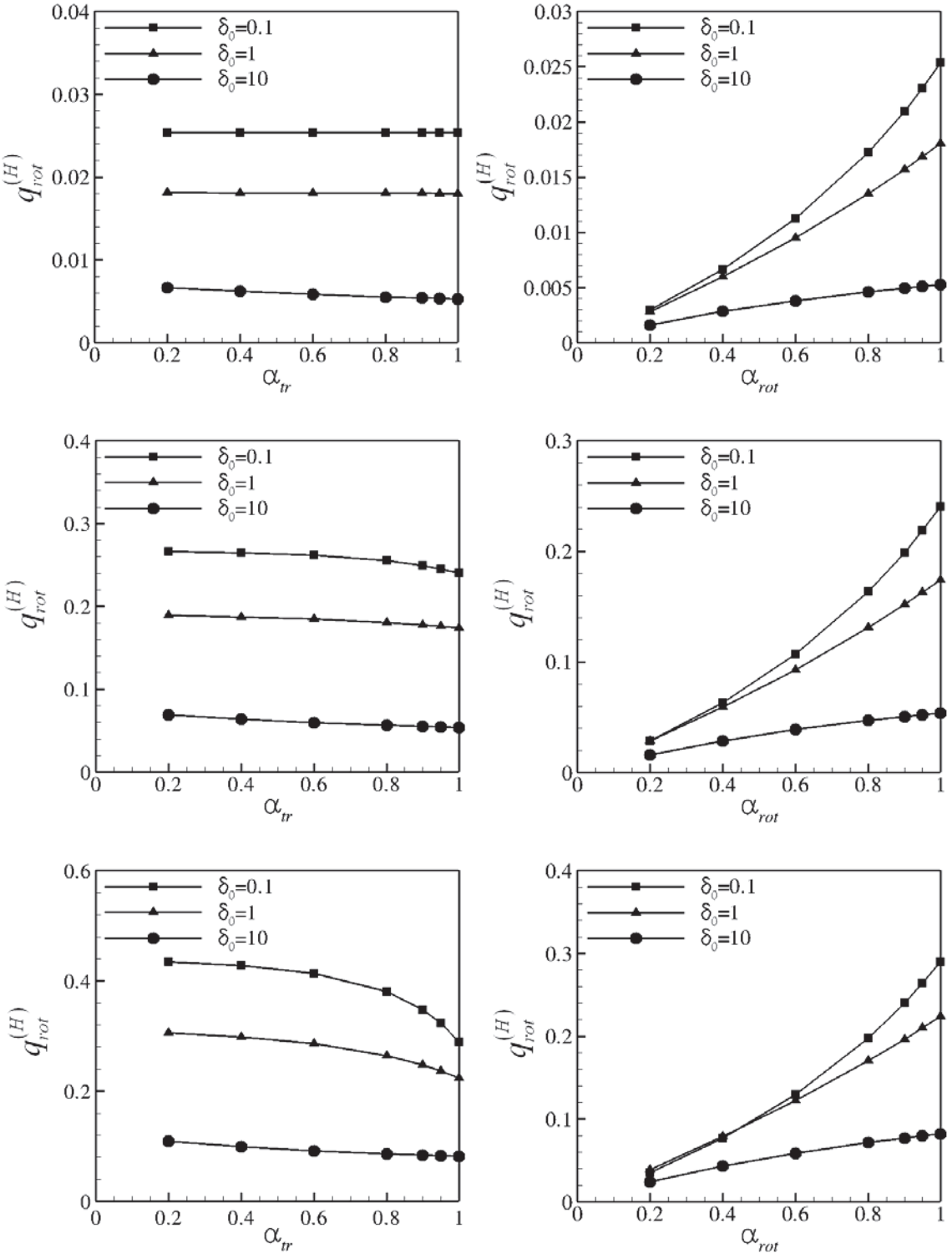

Figure 6: Dimensionless rotational heat flux $q_{rot}^{(H)}$ at the hot plate of a diatomic HS gas ($j=2$, $\mathrm{Pr}=0.71$, $Z=5$) with HS molecules in terms of α_{tr} (left) and α_{rot} (right) for $\delta_0=[0.1,1,10]$ and $T_H/T_C=1.1$ (up), $T_H/T_C=3$ (middle), $T_H/T_C=10$ (down) based on the Holway model.

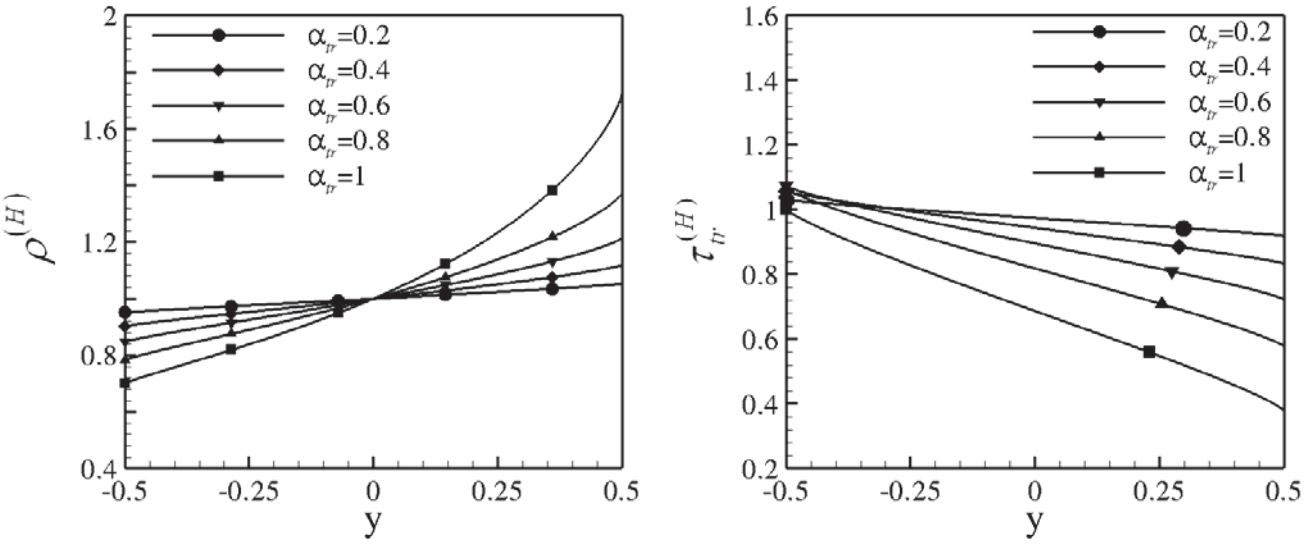

Figure 7: Dimensionless distributions of number density $\rho(y)$ (left) and translational temperature $\tau_{tr}^{(H)}(y)$ (right) of a diatomic HS gas ($j=2$, $\mathrm{Pr}=0.71$, $Z=5$) with $T_H / T_C = 10$ and $\delta_0 = 1$ for various values of α_{tr} with $\alpha_{rot} = 1$, based on the Holway model.

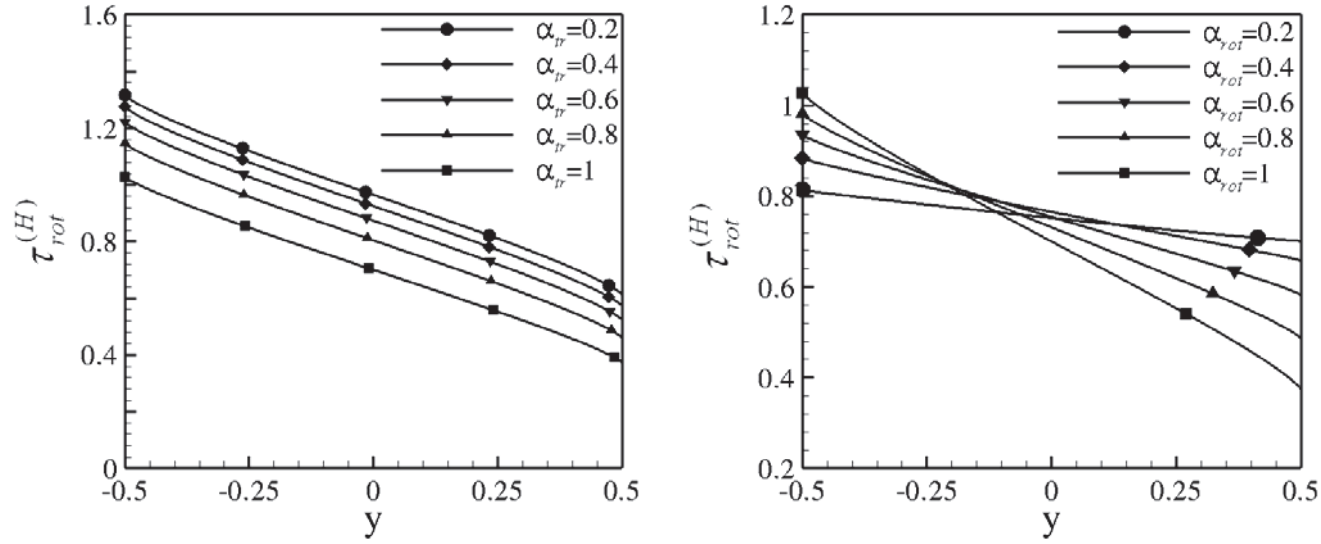

Figure 8: Dimensionless distributions of rotational temperature $\tau_{rot}^{(H)}(y)$ of a diatomic HS gas ($j=2$, $\mathrm{Pr}=0.71$, $Z=5$) with $T_H / T_C = 10$ and $\delta_0 = 1$ for various values of α_{tr} with $\alpha_{rot} = 1$ (left) and α_{rot} with $\alpha_{tr} = 1$ (right), based on the Holway model.

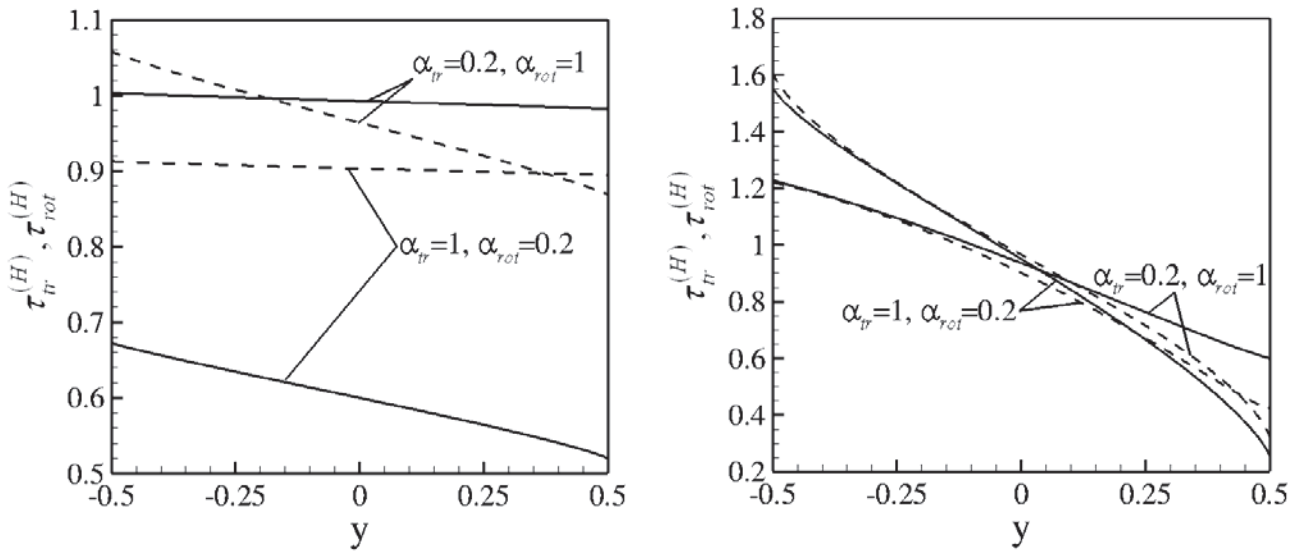

Figure 9: Dimensionless distributions of translational $\tau_{tr}^{(H)}$ (solid lines) and rotational $\tau_{rot}^{(H)}$ (dashed lines) of a diatomic HS gas ($j = 2$, $\mathrm{Pr} = 0.71$, $Z = 5$) with $\alpha_{tr} \neq \alpha_{rot}$ for $T_H / T_C = 10$ and $\delta_0 = 0.1$ (left) and $\delta_0 = 10$ (right), based on the Holway model.

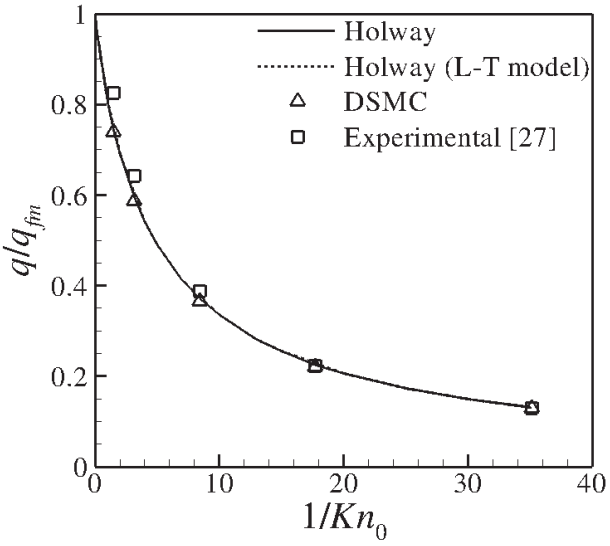

Figure 10: Comparison between the experimental data in [27] and the computational results obtained by the Holway model and the DSMC method (gas: N_2, $\mathrm{Pr} = 0.71$, $Z^{(DSMC)} = 5$, $T_H / T_C = 1.0291$, $T_H = 301.96\,\mathrm{K}$, $\alpha = 0.76$, HS molecules).

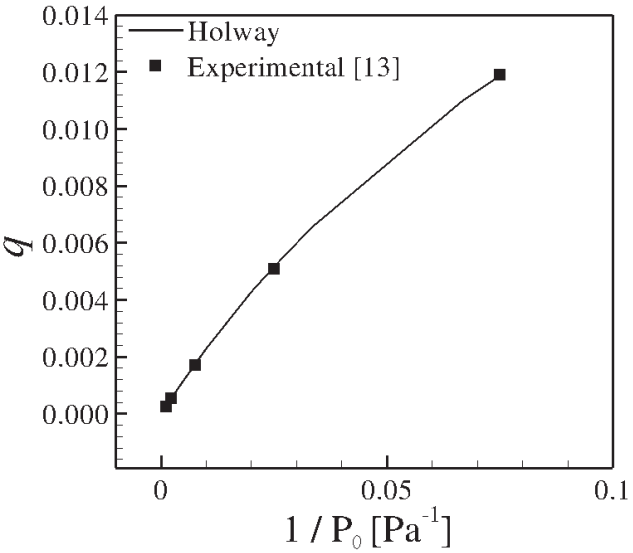

Figure 11: Comparison between the experimental data in [13] and the computational results obtained by the Holway model (gas: N_2, $\mathrm{Pr} = 0.71$, $Z^{(H)} = 5$, $T_H = 303.1\,\mathrm{K}$, $T_H / T_C = 1.052$, $\alpha_C = 0.795$, $\alpha_C = 0.808$, HS molecules).

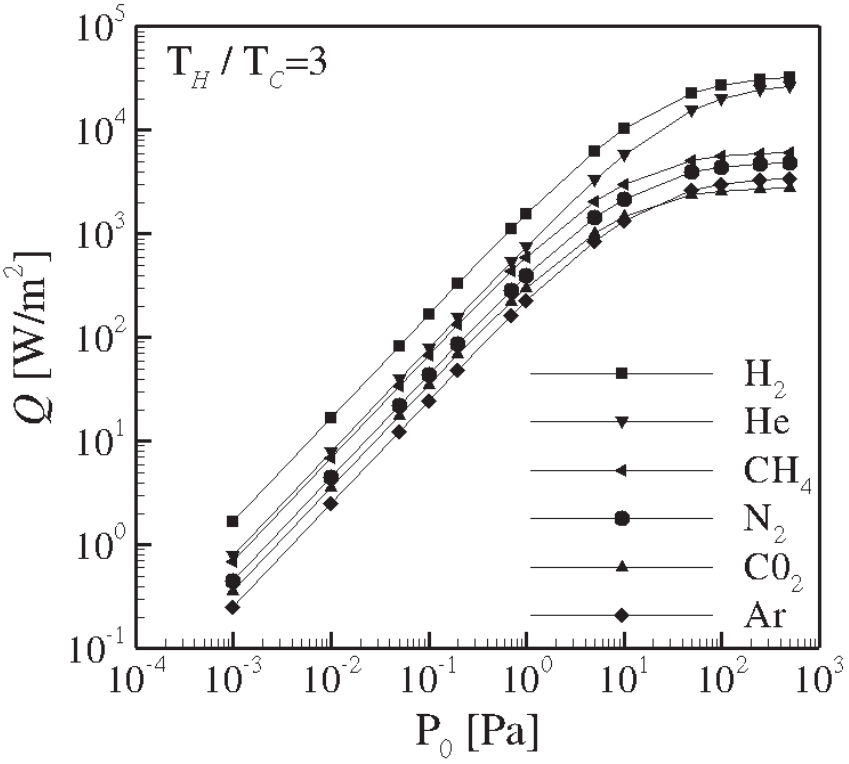

Figure 12: Dimensional heat flux through various gases enclosed between two plates with distance $H = 5\,\text{mm}$ for $T_C = 293\,\text{K}$ and $T_H / T_C = 3$ in terms of the reference pressure obtained by the Holway model ($Z^{(H)} = 5$, VHS model).

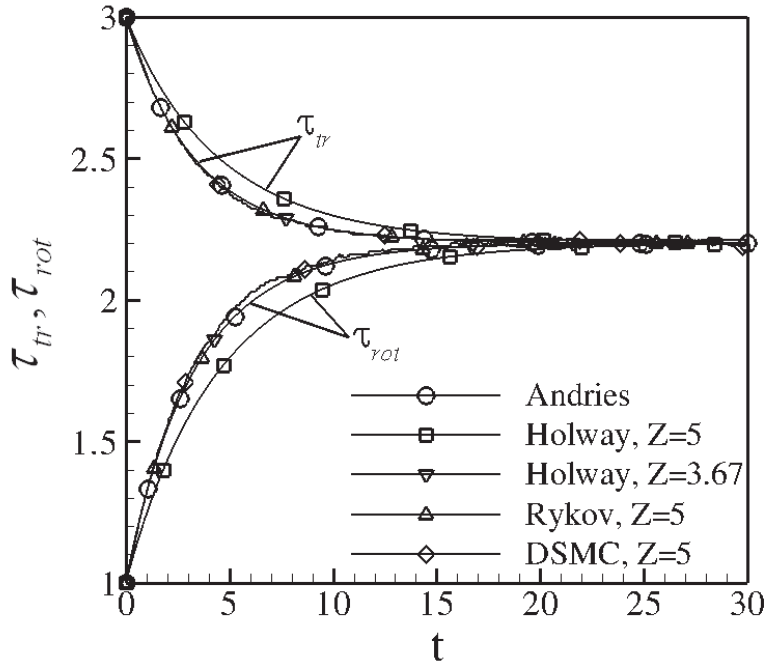

Figure 13: Translational-rotational relaxation in a homogeneous gas.

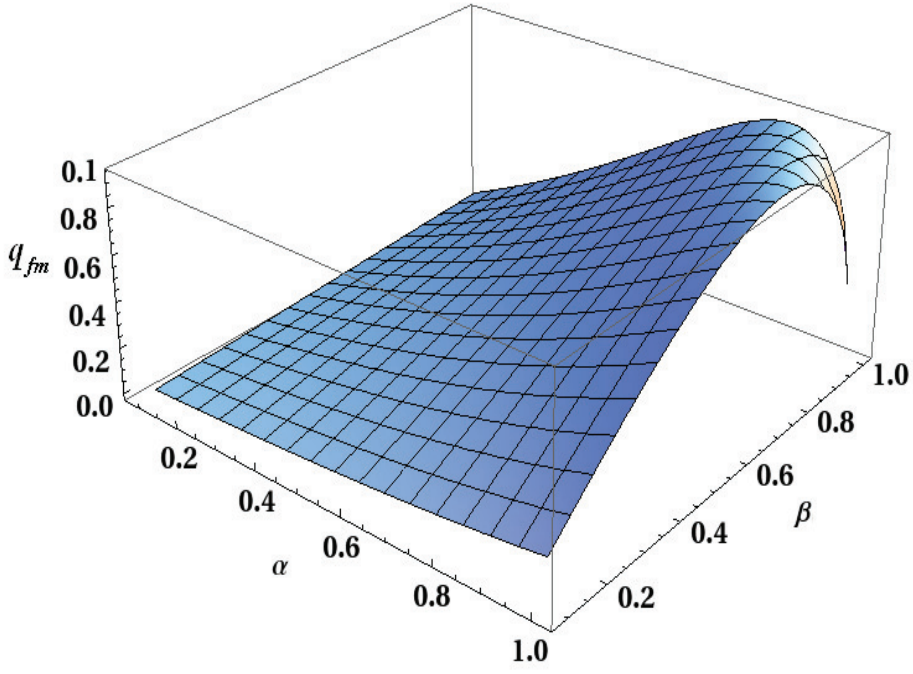

Figure 14: The free molecular total heat flux q_{fm} in terms of the thermal accommodation coefficient α and the normalized temperature difference β.